Cross-species Standardised Cortico-Subcortical Tractography

Stephania Assimopoulos[1], Shaun Warrington[1], Davide Folloni[2,3], Katherine Bryant[4,5], Ali-Reza Mohammadi-Nejad[1,6], Wei Tang[7], Saad Jbabdi[8], Sarah Heilbronner[9], Rogier B Mars[8,10], Stamatios N Sotiropoulos[1,6*]

[1]Sir Peter Mansfield Imaging Centre, School of Medicine, University of Nottingham, UK

[2]Nash Family Department of Neuroscience and Friedman Brain Institute, Icahn School of Medicine at Mount Sinai, New York, NY, USA

[3]Lipschultz Center for Cognitive Neuroscience, Icahn School of Medicine at Mount Sinai, New York, NY, USA

[4]Centre de Recherche en Psychologie et Neurosciences, UMR 7077, CNRS/Université Aix-Marseille, France

[5]Institute for Language, Cognition, and the Brain, CNRS, Université Aix-Marseille, France

[6]NIHR Nottingham Biomedical Research Centre, Queen's Medical Centre, University of Nottingham, UK

[7]Luddy School of Informatics, Computing and Engineering, Indiana University Bloomington, IN, USA

[8]Oxford Centre for Integrative Neuroimaging, University of Oxford, UK

[9]Baylor College of Medicine, Houston, TX, USA

[10]Donders Institute for Brain, Cognition and Behaviour, Radboud University Nijmegen, The Netherlands

[*]Corresponding author. Email: stamatios.sotiropoulos@nottingham.ac.uk

Abstract

Despite their importance for brain function, cortico-subcortical white matter tracts are under-represented in diffusion MRI tractography studies. Their non-invasive mapping is more challenging and less explored compared to other major cortico-cortical bundles. We introduce a set of standardised tractography protocols for delineating tracts between the cortex and various deep subcortical structures, including the caudate, putamen, amygdala, thalamus and hippocampus. To enable comparative studies, our protocols are designed for both human and macaque brains. We demonstrate how tractography reconstructions follow topographical principles obtained from tracers in the macaque and how these translate to humans. We show that the proposed protocols are robust against data quality and preserve aspects of individual variability stemming from family structure in humans. Lastly, we demonstrate the value of these species-matched protocols in mapping homologous grey matter regions in humans and macaques, both in cortex and subcortex.

Keywords

Diffusion MRI, cortico-striatal, amygdalofugal, extreme capsule, external capsule, Muratoff bundle, macaque, tracers

1 Introduction

Function-specific brain activity involves the integration of information from multiple remote brain regions. This integration is enabled by white matter (WM) bundles interconnecting different brain regions (*1, 2, 3, 4*). Of particular interest and importance are bundles connecting cortical areas with deep brain structures. Subcortical structures have important roles in affective, cognitive, motor and social functions (*5, 6, 7*), which emerge through interactions with cortical areas that such connections enable (*8, 9, 10*). Hence, the variability of these connections between individuals has been linked to differences in behavioural traits (*11, 12, 13*). Furthermore, their disruption has been associated with abnormal function and pathology in neurodegenerative and mental health disorders (*14, 15, 16, 17*). In the clinic, individual variability in cortico-subcortical connectivity has been used to assist presurgical planning and predict personalised targets for efficacious interventions (*18*).

Chemical tracer studies in the non-human primate (NHP) brain, have provided, and continue to provide, invaluable insights into cortico-subcortical connections, and neuroanatomy in general (*19*). Examples include tracing of cortico-striatal connections (*20, 21, 8, 22*), amygdalofugal connections (*23*) and thalamo-cortical connections (*24, 20*). Comparative neuroanatomy studies can subsequently explore and translate principles of white matter organisation learnt from NHPs to humans (*25, 22, 26*)). Brain imaging and, in particular, diffusion magnetic resonance imaging (dMRI) tractography (*27*) is a crucial component in these comparative studies and beyond (*28, 29, 30*), allowing non-invasive mapping of these connections in the living human.

Towards this direction, recent dMRI-based frameworks have been developed to map respective white matter bundles ("tracts") across NHPs and humans (*31, 32, 33, 34, 29*). These rely on standardised dMRI tractography protocols, comprising of functionally-driven, rather than geometric, definitions, enabling automated and generalisable mapping of homologous major white matter tracts across species (*31*). These developments have allowed cross-species neuroanatomy studies (*35, 36*) and mapping of connections across humans to study links with brain development, function and dysfunction (*37, 38*). A current limitation of these imaging-based approaches is that they have mainly focused so far on cortico-cortical bundles (with the exception of cortico-thalamic connections).

Tractography protocols for white matter bundles that reach deeper subcortical regions, for instance the striatum or the amygdala, are more difficult to standardise. The relative size and proximity of these bundles, and the white matter complexities and bottlenecks they go through, can make their mapping through dMRI particularly challenging. As a consequence, considerably fewer studies have proposed solutions for their reproducible reconstruction, both within and across primate species, compared to more major cortico-cortical bundles (*39, 40, 31, 41*). Some existing studies have focused on cortico-striatal bundles (*42, 43*), uncinate and amygdalofugal fasciculi (*26*), parts of

the extreme capsule (*44*) and the anterior limb of the internal capsule (*25, 22*). However, these either utilise labour-intensive single-subject protocols (*22, 26*), are not designed to be generalisable across species (*42, 43*), or are based mostly on geometrically-driven parcellations that do not necessarily preserve topographical principles of connections (*40*). We propose an approach that addresses these challenges and is automated, standardised, generalisable across two species and includes a larger set of cortico-subcortical bundles than considered before, yielding tractography reconstructions that are driven by neuroanatomical constraints.

Specifically, we build upon our previous work on FSL-XTRACT (*35, 31, 29*) to propose standardised protocols and an end-to-end framework for automated cortico-subcortical tractography in the macaque and human brain, considering connections between the cortex and the caudate, putamen and amygdala. To this end, we use prior anatomical knowledge from NHP tracers to define new generalisable protocols, including the amygdalofugal tract, the Muratoff bundle and the striatal bundle (external capsule) with its frontal, sensorimotor, temporal and parietal parts, augmenting our previous protocols for hippocampal and thalamic tracts (*31*). Due to their close proximity, we also develop new protocols for the respective extreme capsule parts (frontal, temporal, parietal) and revise previously released protocols (*31*) for the uncinate fasciculus, anterior commissure and fornix.

We demonstrate the mapping of the respective bundles in the human and macaque brain and show that tractography reconstructions follow topographical principles obtained from tracers. We show that the proposed definitions are robust against dMRI data quality and preserve aspects of individual variability stemming from family structure in humans, as reflected by higher similarity of reconstructed tracts in the brains of monozygotic twins compared to non-twin siblings and unrelated subjects. We subsequently demonstrate how these tractography reconstructions can improve the identification of homologous grey matter (GM) regions across species, both in cortex and subcortex, on the basis of similarity of grey matter areal connection patterns to the set of proposed white matter bundles (*1, 35*).

2 Results

Using prior anatomical knowledge from tracer studies in the macaque, we developed new tractography protocols for the macaque brain and subsequently translated them to the human brain. We considered 23 tracts in total (11 bilateral, 1 commissural), which included tracts connecting the cortex to the amygdala, caudate and putamen. Specifically, we developed protocols for the amygdalofugal (AMF) pathway, the sensorimotor, frontal, temporal and parietal parts of the striatal bundle/external capsule (StB_m, StB_f, StB_t, StB_p), and the Muratoff bundle (MB). Due to their proximity, we also developed protocols for the frontal, temporal and parietal parts of the extreme

capsule (EmC_f, EmC_t, EmC_p) (neighbouring to the corresponding external capsule parts), and revised previous protocols for the uncinate fasciculus (UF) (neighbouring to the AMF), the fornix (FX) (output tract of the hippocampus next to the amygdala), as well as the anterior commissure (AC) (Table 1 and Supplementary Table S1).

We used the XTRACT approach (*31*) to define tractography protocols, governed by two principles: (i) protocols are comprised of seed/stop/target/exclusion regions of interest (ROIs) defined in template space, so that they are standardised and generalisable (compared to subject-specific protocols), (ii) ROIs are coarse enough and defined equivalently between macaques and humans to enable the tracking of corresponding bundles across species. Full tractography protocols, and modifications to existing protocols, are described in detail in Methods. Protocols were defined in MNI152 template space for human tractography and F99 space (*45, 46*) for macaque tractography. Additionally, we generalised the macaque protocols to the NIMH Macaque Template (NMT v2) (*47*). For clarity, results shown in the main text use the F99 space protocols. Comparison between results in NMT and F99 space can be seen in Supplementary Figure S3.

***Table 1**: New and Revised Subcortical Protocols.* *The developed subcortical tractography protocols for the macaque and human brain. Protocols for Anterior Commissure, Fornix and Uncinate Fasciculus were revised from (31).*

Tract Name	**Abbreviation**
Amygdalofugal Tract	AMF
Anterior Commissure	AC
Extreme Capsule (frontal)	EmC_f
Extreme Capsule (temporal)	EmC_t
Extreme Capsule (parietal)	EmC_p
Fornix	FX
Muratoff Bundle	MB
Striatal Bundle (sensorimotor)	StB_m
Striatal Bundle (frontal)	StB_f
Striatal Bundle (temporal)	StB_t
Striatal Bundle (parietal)	StB_p
Uncinate Fasciculus	UF

2.1 Subcortical tract reconstruction across species and comparisons with tracers

Using dMRI data from the macaque ($N = 6$) and human brain ($N = 50$) and the defined protocols, we performed tractography reconstructions for all the tracts of interest. Maximum intensity projections of the resultant group-averaged tract reconstructions for the macaque and human are shown colour-coded in Figure 1 (individual tracts can be seen in Supplementary Figure S1). These reveal overall correspondence in the main bodies of tracts across species, whilst capturing differences in (sub)cortical projections.

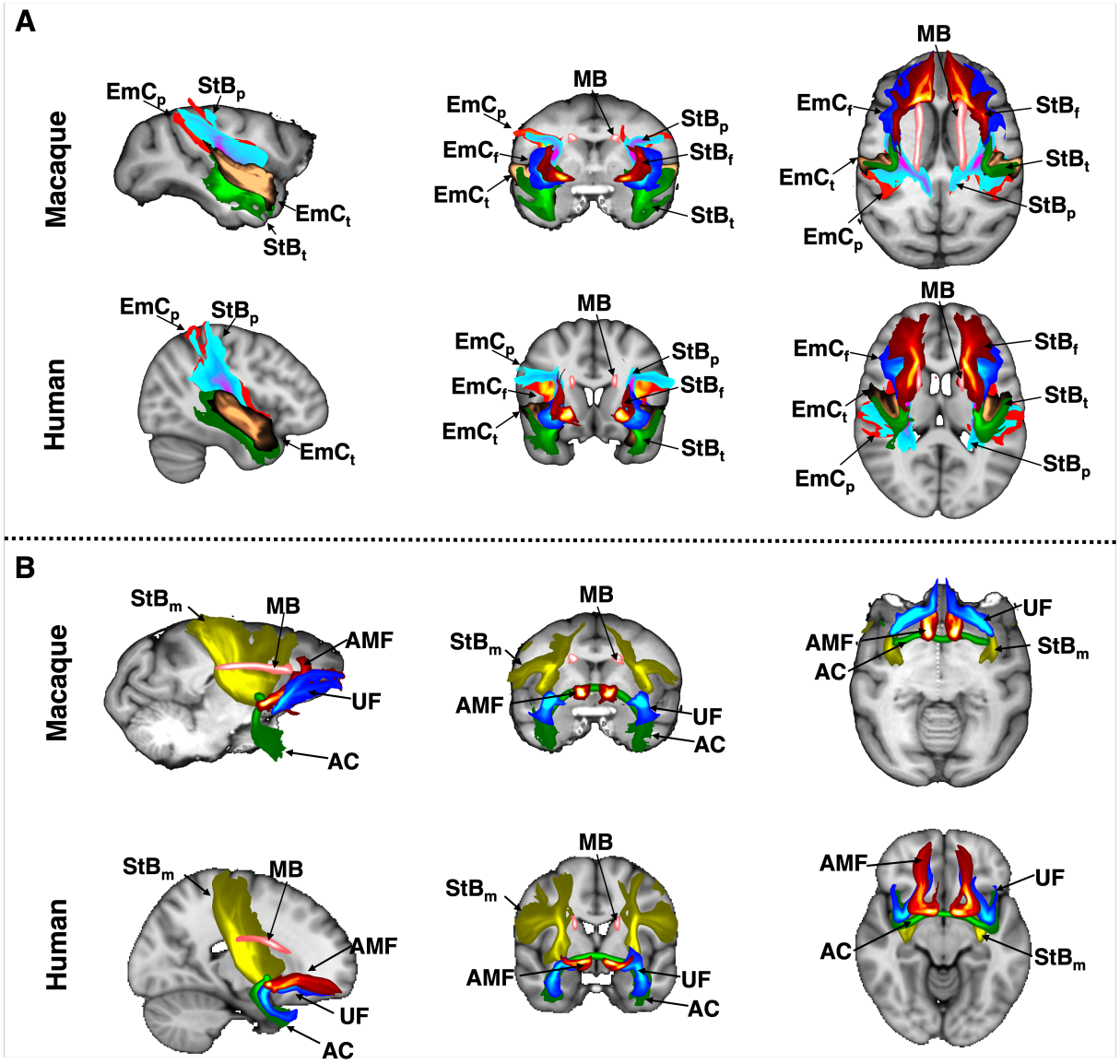

***Figure 1**: **Tractography reconstructions of subcortical bundles in the macaque and human brain using correspondingly defined protocols.** Maximum intensity projections (MIPs) in sagittal, coronal and axial views of group-averaged probabilistic path distributions, for all proposed tractography protocols in the macaque (6 animal average) and human (average of 50 subjects from the Human Connectome Project). All MIPs are within a window of 20% of the field of view centred at the displayed slices. **(A)** Frontal, temporal and parietal parts of the extreme capsule (EmC_f, EmC_t, EmC_p); frontal, temporal and parietal parts of the striatal bundle (StB_f, StB_t, StB_p); and the Muratoff bundle (MB). **(B)** amygdalofugal tract (AMF); anterior commissure (AC); uncinate fasciculus (UF); sensorimotor part of the striatal bundle (StB_m); Muratoff bundle (MB). Path distributions were thresholded at 0.1% before averaging.*

We explored whether white matter organisation principles known from the tracer literature are captured in these tractography reconstructions (*48,49,20,50,51,10*). For instance, the striatal bundle (StB)/external capsule is always medial to the extreme capsule and the Muratoff bundle runs along the head of the caudate nucleus. Figure 2A shows the relative positioning for StB_f, EmC_f and MB bundles. Correspondence between tractography results and tract tracing reconstruction in the macaque can be observed, with their relative positions being preserved. This relative position was preserved in the human tractography results as well. Furthermore, the medio-lateral separation is also observed in the other parts of StB and EmC (i.e. parietal, temporal), as shown in Supplementary Figure S2. Similarly for the amygdalofugal (AMF) bundle (Figure 2B), this runs through the anterior commissure and ventral pallidum, as well as, in its lateral part, over the uncinate fasciculus (UF). We see agreement with respect to these relative positions in both the macaque and human.

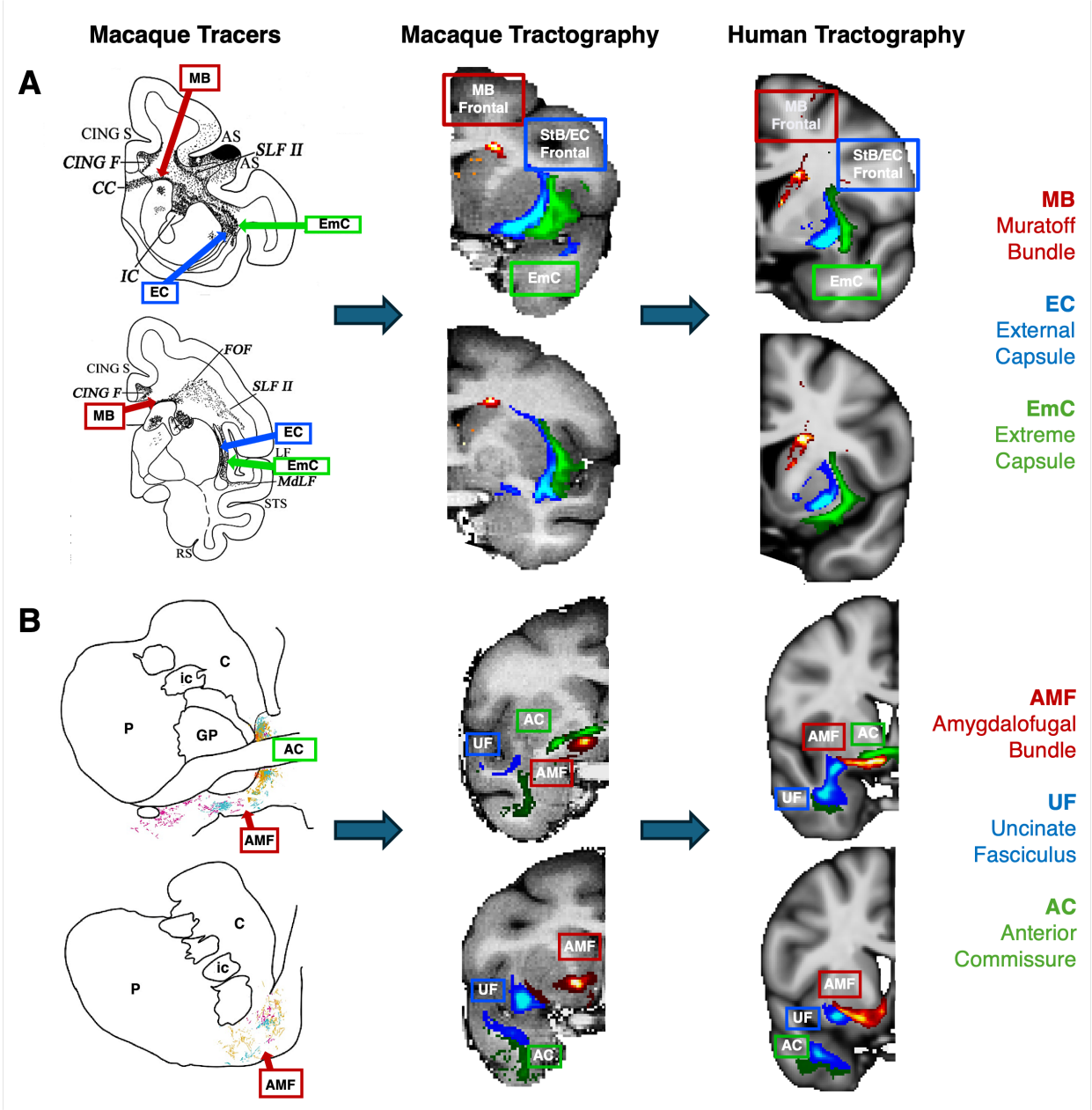

***Figure 2**: **Tractography mirrors tracer patterns in the macaque brain, with similar patterns in the human**. The proposed protocols were first developed in the macaque guided by tracer literature, and then transferred over to the human. Relative positioning of dMRI-reconstructed tracts was subsequently explored against the ones suggested by tracers, with good agreement in both species. **(A)** The dorsal-medial/ventral-lateral separation between the extreme an external capsule (here the frontal parts EmC_f and StB_f shown) is present in macaque tractography, as suggested in the tracer literature. The Muratoff bundle runs along the head of the caudate nucleus. These relative positions are also preserved in the human tractography results. Tracer image modified from (52) with permission. **(B)** Similarly for the amygdalofugal bundle (AMF), which runs under the Anterior Commissure (AC) and over the Uncinate Fasciculus (UF), we see agreement with tracer studies with respect to its location in both the macaque and human tractography (23, 26, 53). Tracer image adapted from (23) with permission. In all examples group-average tractography results are shown.*

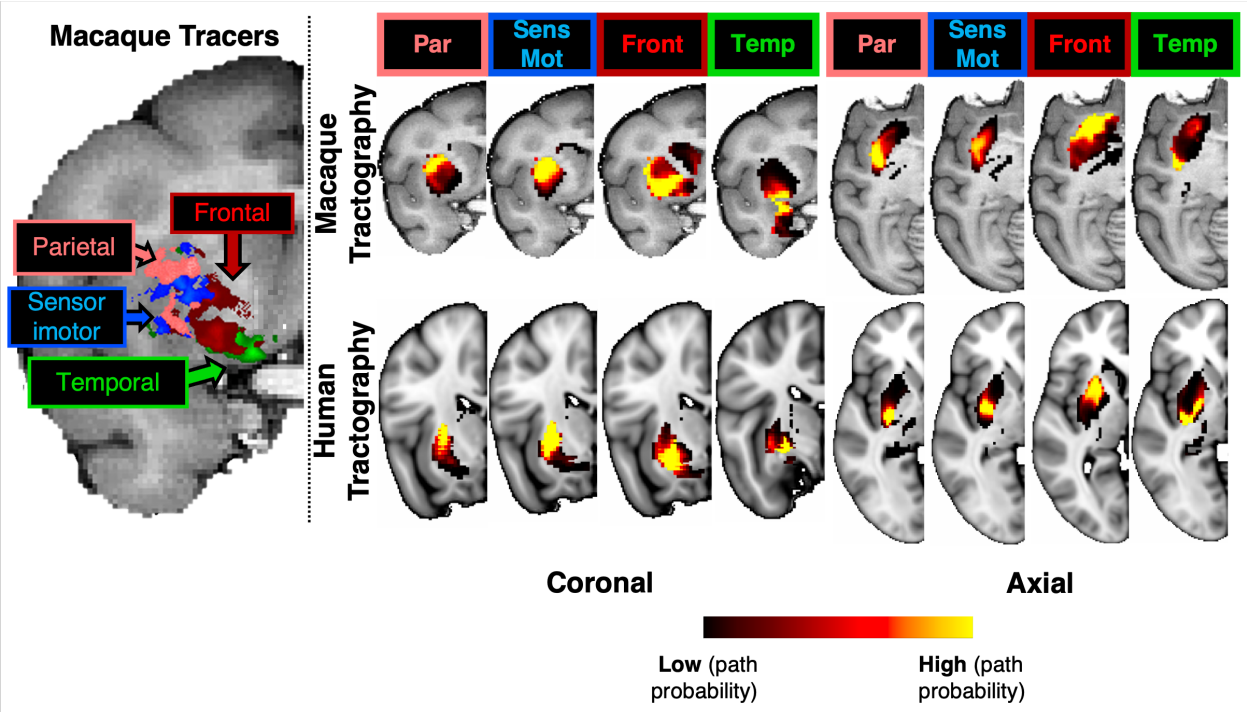

***Figure 3**: Tractography-derived connectivity patterns in the putamen resemble (for both macaque and human) termination sites identified by tracers after injections at different cortical areas (frontal, sensorimotor, parietal, temporal) in the macaque. **Left:** Using macaque tracer data from 78 injections in various parts of the cortex, tracer termination sites in the putamen suggested a pattern based on the distinct cortical origin of the tracer injection sites; moving from the dorsolateral to the ventromedial putamen. **Right:** The path distributions of the different parts of the striatal bundle (StB_f, StB_m, StB_p, StB_t) within the putamen reveal a similar pattern of connectivity to different parts of the cortex, both for macaque (top) and the human (bottom). Coronal and axial views of group-average results are shown for tractography. Cortical areas (Front: frontal cortex, Par: parietal cortex, Temp: temporal cortex, SensMot: Sensorimotor cortex) were obtained from the CHARM1 parcellation (54) in the macaque brain (for both tracers and tractography) and from the Harvard parcellation in the human (55, 56, 49).*

In addition to the main white matter core of the reconstructed bundles, we also explored agreement of the relative connectivity patterns within the striatum between tracers and tractography. Cortical injections of anterograde tracers from different parts of the macaque brain reveal a dorsolateral to ventromedial organisation in the putamen, from parietal to temporal projections (Figure 3). Using the path distribution of the tractography reconstructed StB parts within the putamen, we could obtain a similar pattern in the macaque brain. This also resembled the pattern found in the human brain, as shown in both coronal and axial views.

2.2 Generalisability across data and individuals

We subsequently explored generalisability and robustness of the tractography protocols against NHP template spaces and dMRI data quality. Supplementary Figure S3 shows tract reconstructions in the macaque brain when using the F99 (*45*) vs the NMT (*47*) templates, similar tractography reconstructions for protocols defined in either of the two templates.

To explore performance against data quality, we compared tractography reconstruction in very high-quality high-resolution data from the Human Connectome Project (HCP) (*57, 28*), to tractography in more standard quality data from the UK Biobank dataset (*58*). Supplementary Figure S4 demonstrates the ability to reconstruct all tracts across a range of data qualities, with good correspondence of the main bodies of the tracts in both datasets. We quantified this agreement by calculating the mean Pearson's correlation across the set of new and revised tracts for each unique pair of subjects across and within each of the HCP and UK Biobank (UKB) datasets (Figure 4A). For reference, we performed similar correlations for the original set of XTRACT tracts (*31*) (see Supplementary Table S1 for a list of Original vs New+Revised tracts). Higher correlation was observed within each dataset, but also a sufficiently high correlation between the two datasets. We found similar patterns across datasets both for the original and the new tracts, showcasing that the new protocols behave similarly to the widely-used original XTRACT protocols, across data qualities.

The mean agreement between HCP and UKB reconstructions was lower compared to within-dataset agreements. The two cohorts correspond to different age ranges, with HCP having younger adults than the UKB, which could be contributing to these differences. In addition, this was due to occasionally reconstructing a sparser path distribution in the low-resolution data, particularly for some of the new tracts, as both their relative size and their proximity make them more challenging. This highlights the potential importance of having high-resolution data in tracking white matter bundles in densely-packed areas of higher complexity. It is interesting to note, however, that similar tracts were less/more reproducible between subjects across data qualities. For the lower quality data from the UKB, the tracts with lowest agreement across subjects (4) were the anterior commissure (AC) and the temporal part of the Extreme Capsule (EmC_t), while the highest correlations were for the Muratoff Bundle (MB) and the temporal part of the Striatal Bundle (StB_t). For the higher quality HCP data, the temporal part of the Extreme Capsule (EmC_t) and the Muratoff Bundle (MB) were also the tracts with the lowest/highest correlations across subjects, respectively. Hence, certain tract reconstructions were consistently more variable than others across subjects, which may hint to also being more challenging to reconstruct. Taken together, despite differences, our results suggest all tracts could be reconstructed across both data qualities in a generalisable manner (Supplementary Figure S4).

We subsequently explored whether the proposed protocols preserve aspects of individual variability. We used the family structure in the HCP data to explore whether tract reconstructions from monozygotic twin pairs are more similar compared to tracts obtained from other pairs of siblings or unrelated subjects. As shown in Figure 4B, we found a decrease in pairwise tract similarity going from monozygotic twins, to dizygotic twins and non-twin siblings, and to pairs of unrelated subjects. For reference, we performed the same analysis for the original XTRACT tracts and the same pattern persisted for the new (and revised) tracts, in agreement with previous work (*59, 60, 31*). In each analysis, all pairwise differences were significant (Bonferroni corrected $p \prec 0.05$; following a Mann-Whitney U-Test), with the exception of dizygotic twins compared to non-twin siblings.

Examples of tract reconstructions on individual subjects are shown in Supplementary Figures S6, S7. The figures demonstrate tractography results for subjects corresponding to 10th, 50th and 90th percentile of the distribution of tract correlations to the HCP group average. This ranking was also representative of high, medium and low subject motion across the cohort respectively. Results demonstrate that the expected patterns are preserved for all tracts (MB, AMF, UF, EmC, StB (frontal and parietal parts)). Supplementary Figure S6 shows that even the relative medial-lateral organisation of the StB with respect to the EmC is also maintained across the three individual examples, in agreement with the group average pattern.

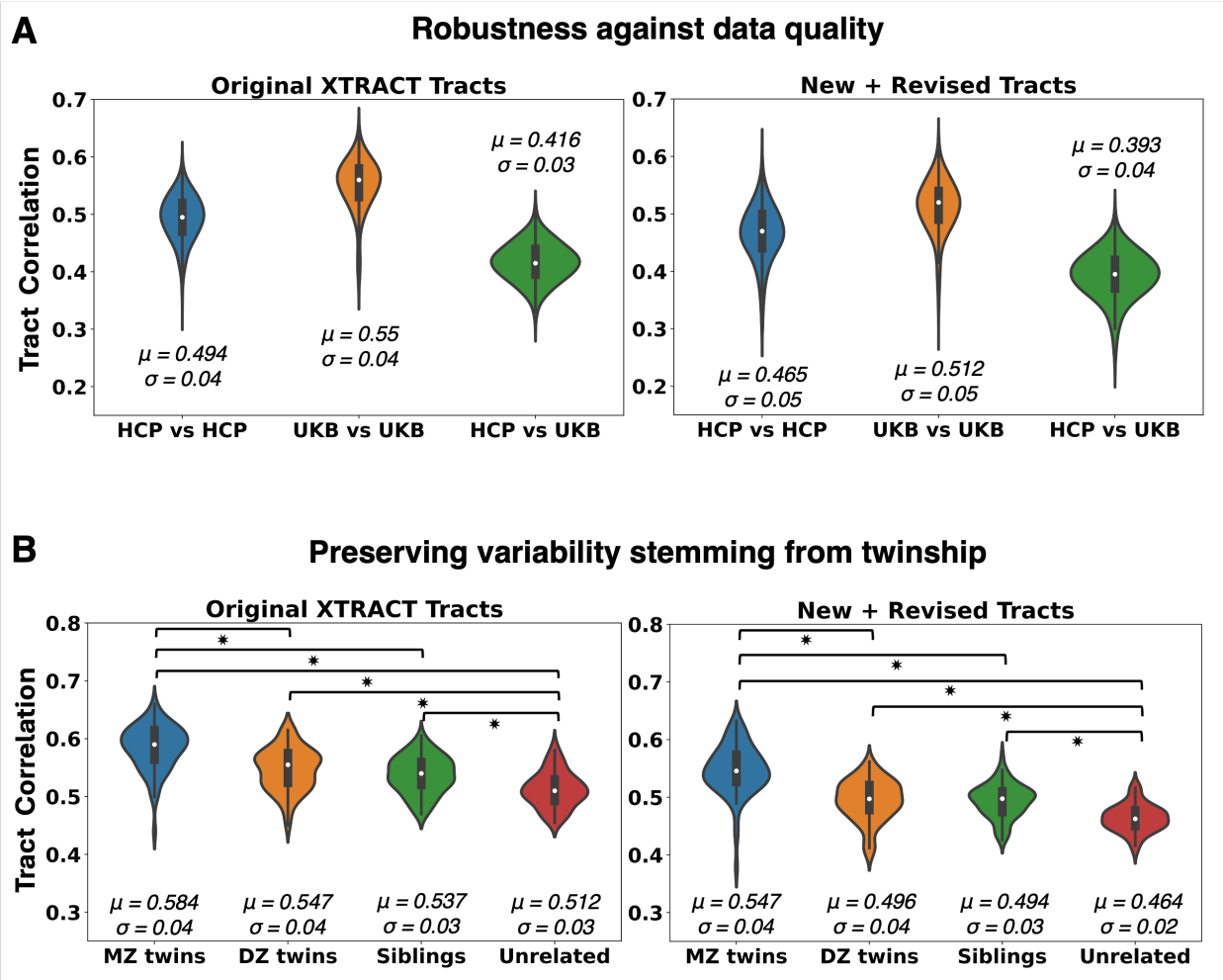

***Figure 4**: Generalisability of proposed tractography reconstructions across data quality and individuals.* *Results for the new subcortical tracts (right column) are shown against reference corresponding results for the original set of XTRACT tracts (left column), which have been widely used (31). (**A**) Tract similarity within and between two in-vivo human cohorts, spanning a wide range of dMRI data quality (HCP: high resolution, long scan time, bespoke setup, UK Biobank (UKB): standard resolution, short scan time, clinical scanner). Violin plots of the average across tracts pairwise Pearson's correlations, between 1,225 unique subject pairs within and across the two cohorts, are shown. Correlations are performed on normalised tract density maps with a threshold of 0.5%. Reported μ is the mean of the correlations across tracts and subject pairs and σ is the standard deviation. (**B**) Tract similarity in twins, non-twin siblings and unrelated subjects. Violin plots of the average across tracts pairwise Pearson's correlations between 72 monozygotic (MZ) twin pairs, 72 dizygotic (DZ) twin pairs, 72 non-twin sibling pairs, and 72 unrelated subject pairs from the Human Connectome Project. Heritable traits are more similar in MZ twins, equally similar in DZ twins and non-twin siblings and more than in unrelated subjects. Asterisk indicates significant pairwise comparisons between groups, as indicated by the brackets.*

2.3 Identifying homologues in cortex and subcortex using tractography patterns

Based on our previous work (*35*), we used the similarity of areal connectivity patterns with respect to equivalently defined white matter tracts across the two species, to identify homologous grey matter regions between humans and macaques. With the addition of the new subcortical tracts we could perform this task for deep brain structures (subcortical nuclei and hippocampus) with considerably greater granularity than before. Figure 5 demonstrates such identification task for five structures in the left hemisphere (caudate, putamen, thalamus, amygdala, hippocampus) using cortico-cortical and cortico-subcortical tracts (sets of tracts defined in Supplementary Table S1). On the left, the regions in the macaque brain with the lowest divergence (highest similarity) in their connectivity patterns to the connectivity patterns of the corresponding human regions are shown in blue. Using only connectivity pattern similarity, these five structures can be matched almost perfectly across the two species. For instance, human putamen (left hemisphere) has more similar connectivity (lower divergence) to macaque putamen (left hemisphere), human thalamus (left hemisphere) to macaque thalamus (left hemisphere), etc. Since we are mapping structures in the left hemisphere using left hemisphere tracts, we observe a low similarity in the contralateral (right) hemisphere, as expected. On the right of Figure 5, this identification is quantified even further, highlighting the value of considering the new tracts. For every human left-hemisphere region (specified on the vertical axis) the boxplot of divergence of connectivity patterns to each of the five macaque deep brain regions (left-hemisphere) is plotted. The best match corresponds to the boxplot with the lowest values (green) and the dashed blue lines show the medians of these boxplots for each case. For reference, the medians of the divergence values when not considering the new subcortical tracts are shown with the red dashed lines, which are overall more flat (with the exception of the hippocampus which has a connectivity pattern strongly driven by the dorsal subsection of the cingulum bundle (CBD), a cortico-cortical tract). It is evident that considering the new tracts provides enhanced contrast between the subcortical structures connectivity patterns, enabling their correct identification. The improvement is thus not in the best match, but in the specificity of the match.

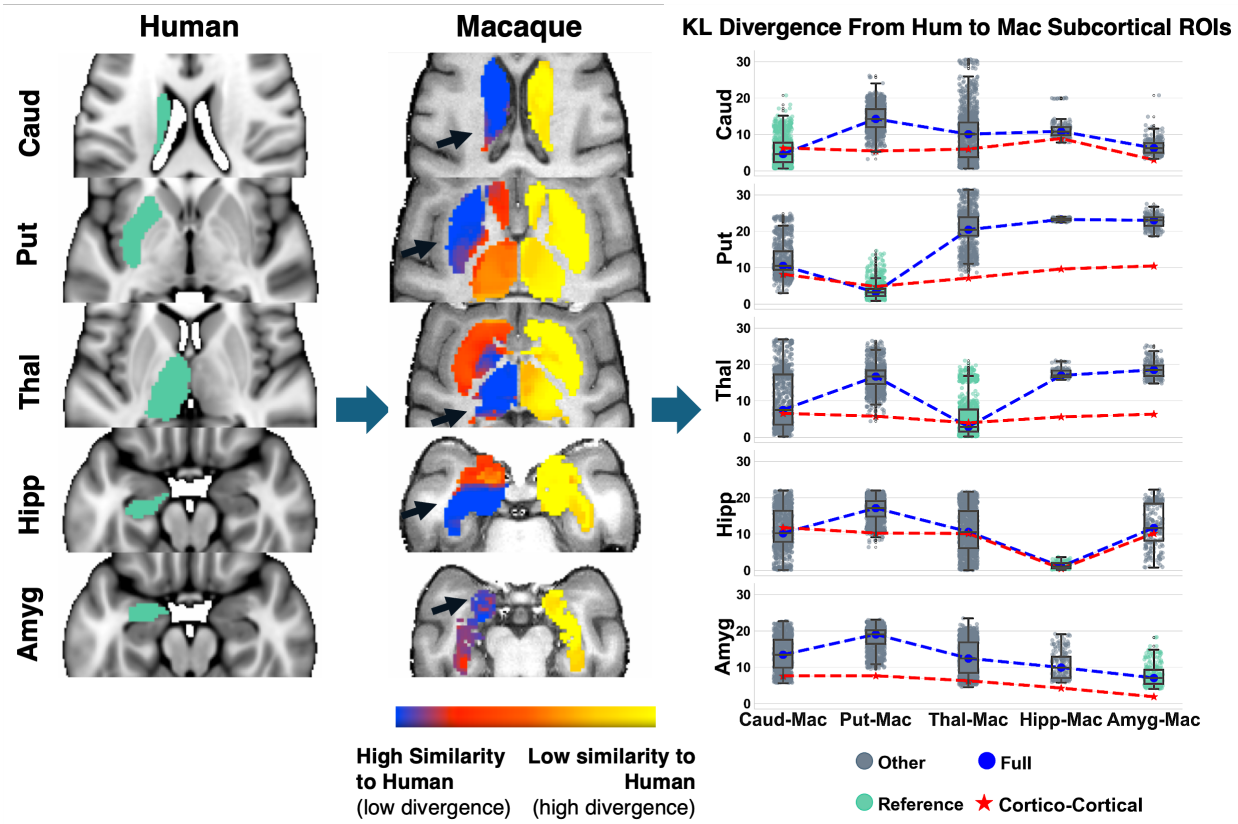

***Figure 5**: **Identifying homologous deep brain structures (subcortical nuclei and hippocampus) across species solely by connectivity pattern similarity, obtained by the new tractography reconstructions.** Using the corresponding tracts in humans and macaques, connectivity blueprints can be calculated. These are GMxTracts matrices, with each row providing the pattern of how a GM location is connected to the predefined set of Tracts (35). **Left:** Starting from the average connectivity blueprints of reference human ROIs (Caud: Caudate, Put: Putamen, Thal: Thalamus, Hipp: Hippocampus, Amyg: Amygdala), Kullback-Leibler (KL) divergence (or inverse similarity) maps can be computed against the connectivity blueprints of deeper subcortical regions in the macaque (**Middle**). The highest connection pattern similarity corresponds to the homologue macaque region of the corresponding human one. **Right**: Boxplots of KL divergence values between reference human regions and the five macaque ones. Blue dashed line corresponds to median KL divergence values when all white matter tracts are considered (both cortico-cortical and the new subcortical ones). Red dashed line corresponds to median KL divergence when using only cortico-cortical tracts. When cortico-subcortical tracts are included vs not, there is increased specificity/contrast in the cross-species mapping of these deeper structures. The boxplot with the lowest median divergence is shown in green in each case, indicating the best matching regions in the macaque to the human reference (i.e. caudate human reference best matches macaque caudate, putamen human reference best matches macaque putamen, etc).*

Having shown increased contrast and specificity in the mapping of deep brain structures, we investigated whether we see a similar effect in the cortex. We selected a set of nearby frontal region pairs to map across the human and the macaque (Figure 6), since a number of the new tracts connect frontal regions to the subcortex. Specifically, we considered the dorsomedial prefrontal cortex ($dmPFC$), the ventromedial prefrontal cortex ($vmPFC$), the rostral orbitofrontal cortex (OFC_r), and the frontal operculum (FOp). These regions were also chosen as they are part of different functional networks (default mode, limbic, and frontoparietal networks), equivalently defined between the macaque and human (*61*).

The prediction from human to macaque is shown in Figure 6A, while the converse prediction from macaque to human is shown in Figure 6B. In each case, we compare the prediction using only cortico-cortical tracts (column 1), using only cortico-subcortical tracts (column 2), and using the full set (column 3) (sets of tracts defined in Supplementary Table S1 - the middle cerebellar peduncle (MCP) was not used in these comparisons). The predicted areas with the highest similarity in connectivity patterns are depicted in blue, while the a priori expected homologue region borders have been outlined in cyan. These results demonstrate benefits when using the subcortical tracts, with mapping of some regions (for instance $vmPFC$ and OFC_r) being improved more than others. However, in general, we observed an increase in cross-species similarity in the corresponding areas of interest, combined with a decrease in similarity everywhere else in the cortex, when we considered cortico-subcortical tracts (columns 2, 3) compared to when we considered cortico-cortical tracts alone (column 1).

Figure 7 provides a further insight into these mappings, by plotting the connectivity patterns of the human regions against the pattern of its identified best match in the macaque brain. As can be observed, despite the relative proximity of these frontal regions, we have distinct patterns across them. With the exception of $dmPFC$, the connectivity patterns of all other regions have major contributions from the frontal striatal bundle, the extreme capsule and the amygdalofugal tract (AMF) and connection patterns to these cortico-subcortical bundles enable better separation of these nearby regions. For instance, $vmPFC$ and $dmPFC$ have both connections through the cingulum bundle, the corpus callosum and the inferior fronto-occipital fasciculus. However, they connect differently to the striatal bundle, the amygdalofugal tract and the anterior thalamic radiation and the addition of these tracts in the connectivity patterns allow the two regions to be better distinguished. The FOp and OFC_r have both relatively strong connection patterns to the uncinate and the inferior fronto-occipital fasciculi, but it is their different pattern of connections to extreme and external capsules and the amygdalofugal tract that enable their better separation.

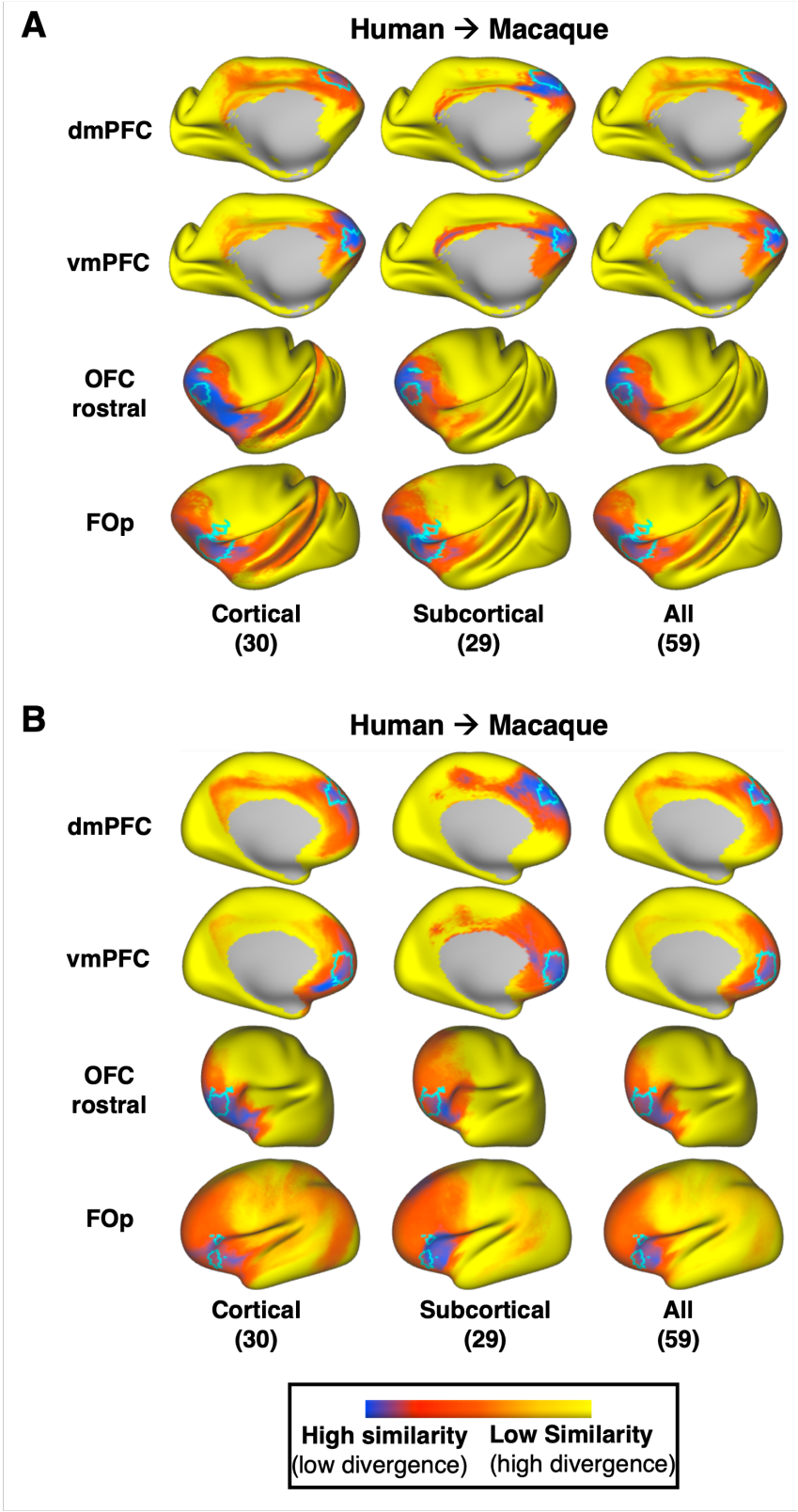
A
Human → Macaque
dmPFC
vmPFC
OFC
rostral
FOp
Cortical
(30)
Subcortical
(29)
All
(59)
B
Human → Macaque
dmPFC
vmPFC
OFC
rostral
FOp
Cortical
(30)
Subcortical
(29)
All
(59)
High similarity
(low divergence)
Low Similarity
(high divergence)

Figure 6

***Figure 6*: Identifying homologous cortical regions across species solely by connectivity pattern similarity, obtained with and without the new tractography reconstructions.** *Two pairs of neighbouring frontal regions were chosen ($dmPFC$: dorsomedial prefrontal cortex & $vmPFC$: ventromedial prefrontal cortex, OFC_r: rostral orbitofrontal cortex & FOp: frontal operculum) and their mapping from human to macaque (**A**) and from macaque to human (**B**) was explored. For comparison, we overlay in cyan the corresponding homologue regions in each species , as defined in (26). **(A)** Kullback-Leibler (KL) divergence maps in the macaque for a given human cortical reference region, (one region per row), representing the similarity in connectivity patterns across the macaque cortex to the average pattern of the human reference region. KL divergence maps are calculated using cortico-cortical (1st column), cortico-subcortical 2nd column) and all tracts (3rd column) to highlight the effect of the cortico-subcortical tractography reconstructions in the prediction. Subcortical tracts provide larger benefits for the prediction of $vmPFC$ and OFC_r, increasing specificity with respect to the expected borders. **(B)** Same as in **A**, but using macaque regions as reference and making predictions on the human cortex. KL divergence maps in the human for a given macaque cortical region, representing the similarity of connectivity pattern across the human cortex to the average pattern of the reference macaque region. Overall, in both species, an increased similarity to the reference regions in the homologue areas and decreased similarity across the rest of the cortex is observed, when cortico-subcortical tracts are considered (2nd or 3rd column).*

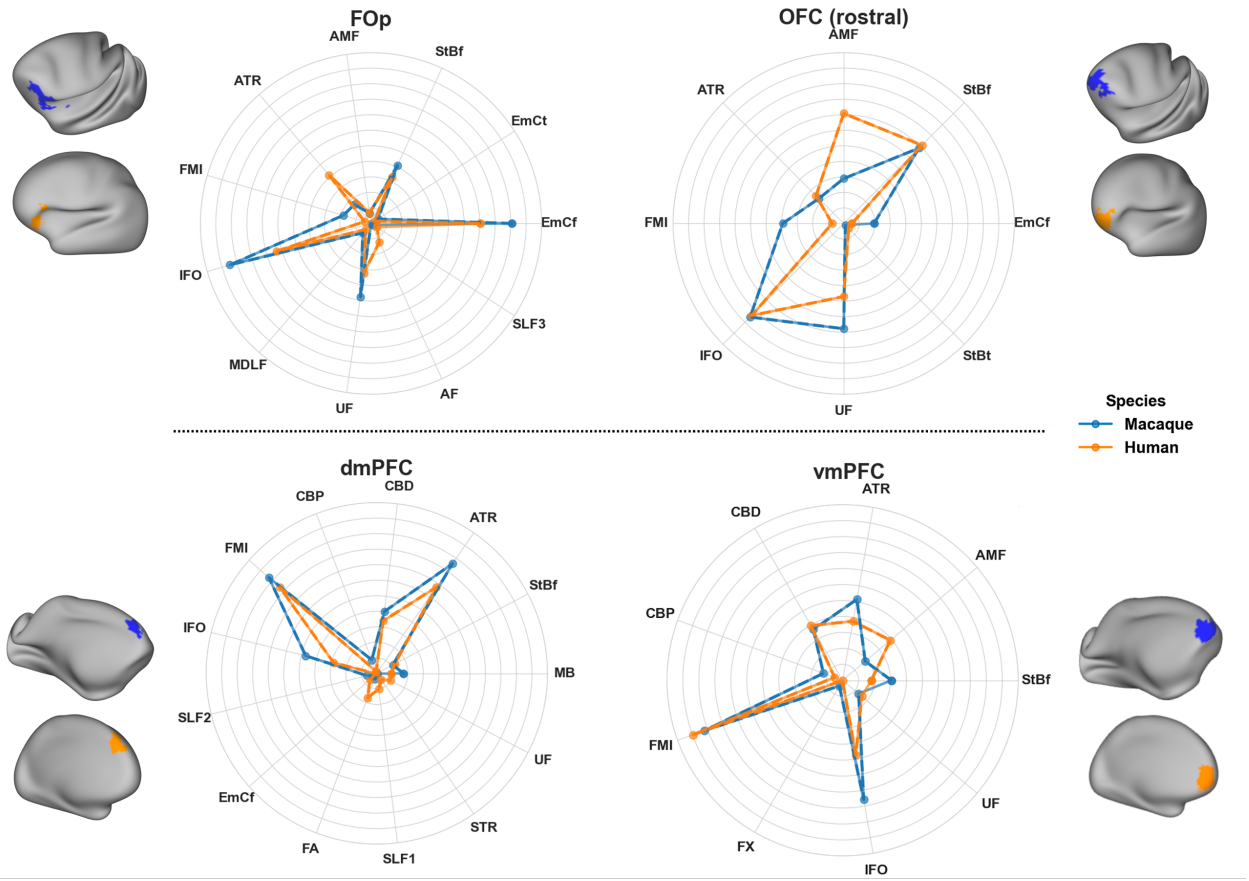

Figure 7: Connectivity patterns for neighbouring frontal region pairs, showing distinct cortico-subcortical tract contributions in macaque and human. *Considered regions are the same as in Figure 6A, i.e. FOp: frontal operculum, OFC_r: rostral orbitofrontal cortex, $dmPFC$: dorsomedial prefrontal cortex, $vmPFC$: ventromedial prefrontal cortex. Reference regions were chosen in the human cortex, shown in orange, and obtained from (26). The best matching region across the whole macaque cortex was identified by the minimum KL divergence in connectivity patterns (thresholded at the 7th percentile in each case) and is shown in blue. Average connectivity patterns for the reference and best-matching regions are depicted using the polar plots. For each region, similarities in the connectivity patterns between the macaque and human can be observed, with the new cortico-subcortical bundles contributing to these patterns. For instance, FOp has a strong connection pattern involving EMC_f and UF and moderately StB_f and AF, while its neighbouring OFC_r has a stronger pattern involving StB_f and UF, compared to EMC_f. These differences are preserved across both species.*

3 Discussion

We introduced standardised dMRI tractography protocols for delineating cortico-subcortical connections between cortex and the amygdala, caudate, putamen and the hippocampus, across humans and macaques. Building upon our previous work (*35, 31*), which already provided protocols for cortico-thalamic radiations, and guided by the chemical tracer literature in the macaque, we devised

the new protocols first for the macaque and then extended to humans. We demonstrated that our reconstructed tracts preserve topographical organisation principles, as suggested by tracers (*62, 8, 63*).

As outlined in (*43*), tractography reconstructions can be highly accurate if information about where pathways go, and where they do not go is available. This is the philosophy behind the proposed protocols, which provide this type of constraints across different bundles. At the same time these constraints are relatively coarse so that they are species-generalisable. We found that the proposed approaches yield tractography reconstruction across a range of datasets and respect individual similarities stemming from twinship. We further assessed the efficacy of these protocols in performing connectivity-based identification of homologous cortical and subcortical areas across the two species (*35, 36, 38*).

Mapping white matter tracts that link cortical areas with deep brain structures (subcortical nuclei and hippocampus), as done here, enhances capabilities for studying neuroanatomy in many contexts, from evolution and development, to mental health and neuropathology. As one of the (evolutionarily) older brain structures, the subcortex modulates brain functions including basic emotions, motivation, and movement control, providing a foundation upon which the more complex cognitive abilities of the cortex could develop and evolve (*62, 64, 8, 65, 66*). This modulatory function is mediated via white matter bundles (*8, 9*). Consequently, their disruption is linked to abnormal function and pathology, in mental health, neurodegenerative, and neurodevelopmental disorders (*15, 67, 17*). For example, in depression, fronto-thalamic (*68*), cortico-amygdalar (*69, 70*), and cortico-striatal (*71*) connectivity changes have been reported, while in schizophrenia there are associated fronto-striatal (*72*) and hippocampal connectivity (*73*) changes. In Parkinson's there is impairment in fronto-striatal connectivity (*74, 75, 76, 77*), while fronto-thalamic and cingulate connectivity are impaired in Alzheimer's disease (*75, 78*). Connectivity between the frontal lobe and the amygdala, thalamus, and striatum, as well as cingulum connectivity are impaired in obsessive compulsive disorder (OCD), autism spectrum disorder (ASD), and attention deficit hyperactivity disorder (ADHD) (*79, 69, 14, 80*). Therefore, reconstructing connectivity of these deep brain structures (striatum, thalamus, amygdala, hippocampus) in a standardised manner, as enabled by our proposed tools, allows for further investigation into a wide range of disorders.

In addition, tractography of connections linking to/from deep brain structures has been used or proposed for guiding neuromodulation interventions, for example, deep brain stimulation (DBS) (*81, 82*) or repetitive transcranial magnetic stimulation (rTMS) (*67*). DBS can inherently target subcortical structures and connectivity of subcortical circuits can be used to identify efficacious stimulation targets (*83, 18*). rTMS on the other hand modulates subcortical function indirectly by targetting the structurally connected cortical areas. For example, dmPFC has been targetted to modulate the reward circuitry, in cases of anhedonia, negative symptoms in schizophrenia and major depression disorder (MDD) (*84, 85, 86*), while the vmPFC has been used as a target

to modulate the prefrontal-striatal network (part of the limbic system) and regulate emotional arousal/anxiety (*87, 88, 89*). Our results show a good mapping across species of both these cortical regions with specificity in their connectional patterns . Additionally, the motor cortex has been used as target to modulate cortico-striatal connectivity in general anxiety disorder (*90, 91*). We thus anticipate that having a standardised set of tracts linking the striatum, the hippocampus, the amygdala and the thalamus (all potential sites for stimulation) to specific cortical areas can assist the planning of interventions.

Our cross-species approach naturally lends itself to the study of evolutionary diversity. A number of comparative studies have revealed differences and similarities when comparing brain connectivity between humans and non-human primates (*92*), including macaques (*35, 38*) and chimpanzees (*93*). Our work naturally extends these efforts and provides new tools for studying this diversity in deeper structures and subcortical nuclei. The ever increasing availability of comparative MRI data (*34, 94*) allows the definition of similar protocols in more species, such as the gibbon (*33, 95*) or the marmoset monkey, and even across geometrically diverse brains depicting different stages of neurodevelopment (e.g. neonates vs adults) enabling concurrent studies of phylogeny and ontogeny (*38*)).

Our protocols have been developed and tested using FSL-XTRACT, but, in principle, are not specific to FSL. We have not evaluated performance with other tools, but these standard space protocols could be translated into other tractography approaches. As described before, the protocols are recipes with anatomical constraints, including regions to which the corresponding white matter pathways connect and regions they do not, constructed with cross-species generalisability in mind. Caution may be needed, however, if applying such protocols for segmenting whole-brain tractograms, as these can induce more false positives than tractography reconstructions from smaller seed regions and may require stricter exclusions.

Despite the potential demonstrated in this work, our study has limitations. As this is the first endeavour of this scale to map cortico-subcortical connections in a standardised manner and across two species, it is not exhaustive. Tracts linking the cortex to the striatum were prioritised as they are of increased relevance in human development and disease. However, expanding to include more tracts targetting other structures would provide a more holistic view. Our protocols were developed in the adult human brain. Future work will translate them to the infant brain (expanding on previous work (*38*)) to interrogate cortico-subcortical connectivity across development. Tractography validation is a challenge, as is validation for any indirect and non-invasive imaging approach. We explored and demonstrated generalisability of the proposed protocols, both within and across species. We also showed how the imaging-based reconstructions follow topographical organisation principles suggested by tracers.

4 Methods and Materials

4.1 Tractography protocols

Guided by tract tracing and neuroanatomy literature, we devised tractography protocols for 18 subcortical bundles (nine bilateral - Table 1) using the XTRACT approach (*31*). We also revised protocols for three more bundles (2 bilateral, 1 commissural), compared to their original version (*31*). All protocols followed two principles: i) comprised of seed/stop/target/exclusion regions of interest (ROIs) defined in template space, so that they are standardised and generalisable, ii) ROIs defined equivalently between macaques and humans to enable tracking of corresponding bundles across species. The human protocols were defined in MNI152 space. The macaque protocols were defined in F99 and also in NMT space.

The tracts included the amygdalofugal tract (AMF), the uncinate fasciculus (UF), anterior commissure (AC), sensorimotor, temporal, parietal and frontal parts of the striatal bundle (StB) / external capsule (EC), Muratoff bundle (MB)/subcallosal fasciculus, as well as the extreme capsule (EmC) parts that run close to the putamen connecting the insula to the frontal, temporal and parietal cortices. All XTRACT tracts (Original, Revised and New) are summarised in Supplementary Table S1.

Detailed protocol definitions are presented below and summarised in Figure 8 (for completeness, the previously published thalamic radiations from (*31*) are presented in Supplementary Materials). Briefly, the AMF and UF protocols are a standard-space generalisation of the individual subject-level protocols presented in (*26*). For the remaining protocols, we first devised them in the macaque guided by tract tracer literature. Specifically, the approach we took was to first identify anatomical constraints from neuroanatomy literature for each tract of interest independently, derive and test these protocols in the macaque. Thus, each devised protocol included a unique combination of anatomically defined masks (based on literature descriptions of the tracts), delineated in standard macaque space (F99). We then developed corresponding protocols in the human using correspondingly defined landmarks (delineated in standard MNI space). We optimised in an iterative fashion based on two criteria: (1) the protocols generalise well to humans, and (2) when considering groups of bundles, the generated reconstructions follow topographical principles known from tract tracing literature.

We modified existing XTRACT protocols to improve their specificity in the subcortex. Specifically, we developed a new uncinate fasciculus (UF) protocol based on the protocol presented in (*26*). We also modified the anterior commissure (AC) protocol to improve temporal lobe projections and slightly enhance projections to the amygdala, and modified the fornix (FX) one to reduce amygdala projections by placing an exclusion in the amygdala.

Given the proximity of the newly defined tracts, we evaluated the new protocols against their ability to capture patterns known from the tracer literature. These included relative positioning of each tract with respect to neighbouring tracts (Figure 2) and topographical organisation of certain bundle terminals within subcortical nuclei (Figure 3).

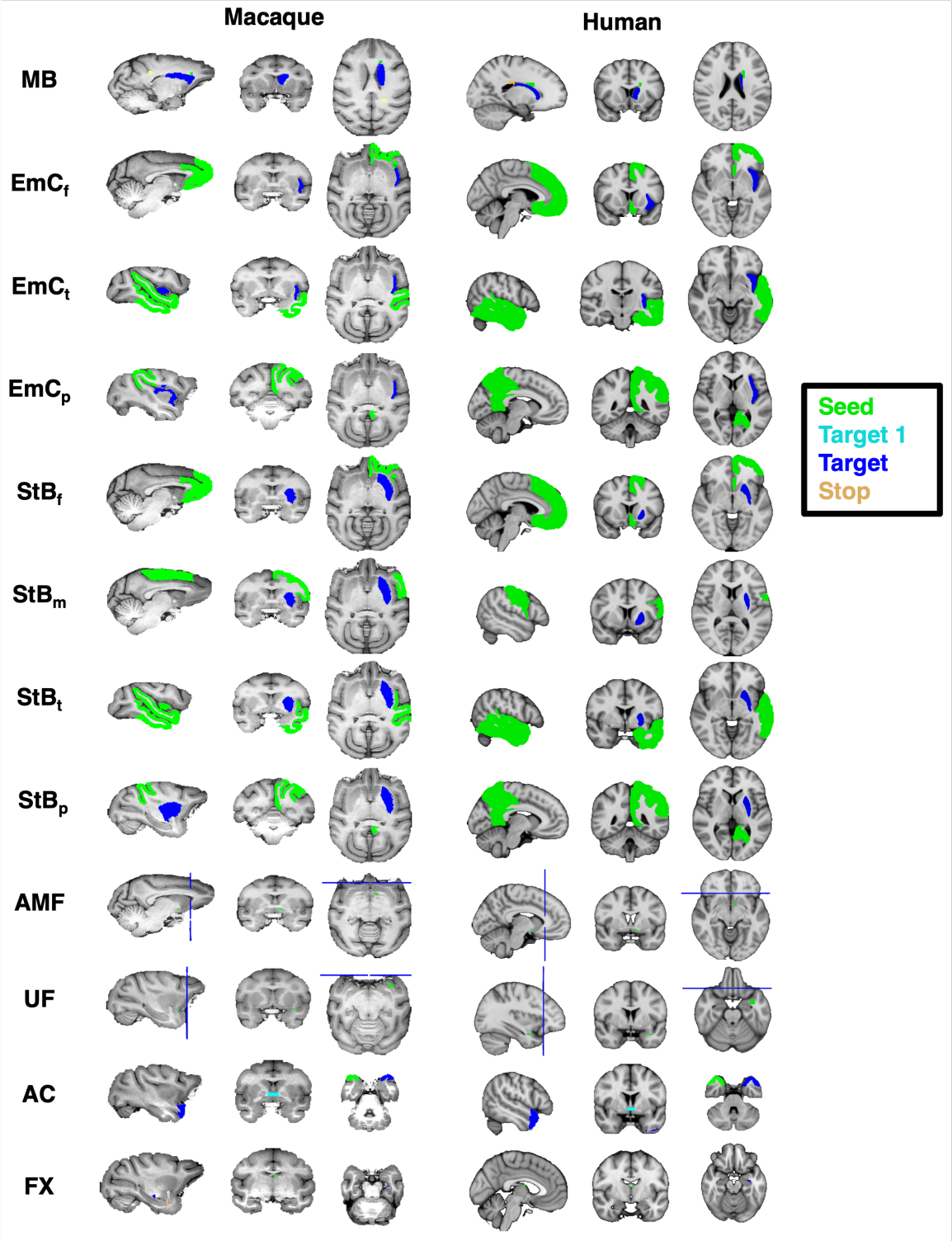

***Figure 8*: Corresponding tract protocol definitions across species.** *Protocol definitions for all new (and revised) tracts in the human and macaque. Protocols were first designed in the macaque brain guided by macaque tracer literature, and then transferred over to the human. Colour-coded regions depict the seed, target and stop masks. Exclusion masks are not shown for ease of visualisation.*

4.1.1 New protocol definitions

Amygdalofugal Pathway (AMF): We derived generalisable template-space protocols to reconstruct the limbic-cortical ventral amygdalofugal pathway, following the subject-specific protocols in (*26*). The amygdalofugal pathway (AMF) courses between the amygdala and the prefrontal cortex (PFC), running alongside the uncinate fasciculus (UF) medially and finally merging with the UF in the posterior orbitofrontal cortex (OFC). As in (*26*), the seed included voxels with high fractional anisotropy in an anterior-posterior direction in the sub-commissural white matter. We used a target covering all brain at the level of caudal genu of the corpus callosum (same target as in the revised UF protocol, described further below). Exclusions include an axial plane through the UF, the internal and external capsules, the corpus callosum, the cingulate, the Sylvian fissure, the anterior commissure, the fornix, and a large coronal exclusion covering all brain dorsal to the corpus callosum and extending inferiorly to the frontal operculum and insula at the level of the middle frontal gyrus.

Striatal Bundle (StB_f, StB_m, StB_p, StB_t): The striatal bundle (StB), is a bundle system that connects the cortex to the striatum, and joins the external capsule (EC). Although terminations reach both the caudate and the putamen, it primarily terminates in the putamen (*48, 49, 10*). Here we defined protocols for bundles that connect the putamen with frontal (including anterior cingulate) lobe, sensorimotor cortex, parietal and temporal lobes. For all parts, we used the putamen as the target. For StB_f, the OFC, PFC, ACC and frontal pole made up the seed. For StB_m, the primary sensorimotor cortex (M1-S1) were used as seeds. For StB_t and StB_p, the temporal and parietal lobes were respectively used as a seed. The exclusion masks shared many commonalities but also had differences. For all parts, exclusions included a midsagittal plane, the subcortex, except for the putamen, as well as the occipital lobe. For each of the parts, we additionally excluded the seeds for every other StB bundle.

Muratoff Bundle (MB): The subcallosal fasciculus tract (as called in human neuroanatomy) or Muratoff bundle (as called in non-human animal neuroanatomy) (*48, 51*) is a complex system of projection fibres which runs beneath the corpus callosum, above the caudate nucleus at the corner formed by the internal capsule and the corpus callosum (*42*). Although terminations reach both the caudate and the putamen, it primarily terminates in the caudate head (*48, 42, 51*). As its cortical projections are challenging to capture and isolate using tractography, we defined a protocol for the major core of the bundle. We used a seed in the white matter adjacent to the caudate head and a target in the white matter adjacent to the caudate tail. A stop mask was used beyond the target in the white matter above the target. Exclusions included the contralateral hemisphere, the subcor-

tex (except for the caudate head), the brainstem, the parietal, occipital, frontal and temporal cortices.

Extreme Capsule (EmC_f, EmC_p, EmC_t): The extreme capsule is a major association fascicle that carries association fibres between frontal-temporal and frontal-parietal, as well as these areas and the insula (*49*). It lies between the claustrum and the insula, with the claustrum being considered the boundary between the EmC and the external capsule (EC) (*10*). We defined protocols connecting the insula to frontal, parietal and temporal cortices. For all parts we used the insula as the target, while for seeds we used the same seeds as for the corresponding StB parts. Hence, for the EmC_f protocol the frontal pole was used as the seed. For EmC_p, the parietal lobe was a seed, and for EmC_t the temporal lobe was a seed. Exclusions for all EmC parts included the contralateral part of the brain, the subcortex, as well as the occipital lobe, and lateral parts of the somatosensory and motor cortices. In addition, for each subdivision, the exclusion mask also included the seed mask for every other subdivision.

4.1.2 Revisions to previous XTRACT protocols

Uncinate Fasciculus (UF): The UF lies at the bottom part of the extreme capsule, curving from the inferior frontal cortex to the anterior temporal cortex. Given the neighbouring bundles that were newly defined, we took a new approach to the UF compared to the original XTRACT implementation (*31*), now following the principles of (*26*). Briefly, we used an axial seed in the white matter rostro-laterally to the amygdala in the anterior temporal lobe. A target covered all brain at the level of caudal genu of the corpus callosum. Exclusions included the basal ganglia, a coronal plane posterior to the seed, the corpus callosum, the cingulate, the Sylvian fissure, the anterior commissure, and a large coronal exclusion covering all brain dorsal to the corpus callosum and extending inferiorly to the frontal operculum and insula at the level of the middle frontal gyrus. This implementation provided improved connectivity to the dorsal frontal cortex and aided separability with respect to neighbouring white matter bundles.

Anterior Commissure (AC): Compared to original XTRACT protocol, we entirely re-worked the AC protocol. Previously, the mid-line main body of the AC was the seed with targets either side and stops at the amygdala. Now, we use a temporal pole as the seed, the main body of the AC as a waypoint and the contralateral temporal pole as the final target. For the human, we use the Harvard-Oxford temporal pole ROI (*56*). For the macaque, we use the CHARM temporal pole ROI (*54*). The temporal pole seed/target pair are flipped and tractography is repeated, taking the average of runs. Compared to the previous version, this protocol provides greater symmetry in resultant reconstructions and greater connectivity to the poles of the temporal cortex, as suggested

in the literature (*96, 97, 98, 10*), and slightly enhanced connectivity to the amygdala.

Fornix (FX): For the FX, a main output tract of the hippocampus, we have added an exclusion mask to the amygdala to prevent FX leakage to the amygdala, thus providing a cleaner FX compared to the original XTRACT implementation (*31*). For the human protocol, we used the Harvard-Oxford amygdala ROI (*55*). For the macaque, we used the SARM amygdala ROI (*99*).

4.2 Data

4.2.1 *Macaque MRI data*

We used six high quality ex-vivo rhesus macaque dMRI datasets, available from PRIME-DE (*100*). As described in (*35, 31*), these were acquired using a 7T Agilent DirectDrive console, with a 2D diffusion-weighted spin-echo protocol with single-line readout protocol with 16 volumes acquired at b=0 s/mm^2, 128 volumes acquired at b=4000 s/mm^2, and a 0.6 mm isotropic spatial resolution.

4.2.2 *Human MRI data*

We used high quality minimally preprocessed (*101*) in-vivo dMRI data from the young adult Human Connectome Project (HCP) (*57, 28*). The HCP data were acquired using a bespoke 3T Connectom Skyra (Siemens, Erlangen) with a monopolar diffusion-weighted (Stejskal-Tanner) spin-echo echo planar imaging (EPI) sequence with an isotropic spatial resolution of 1.25 mm, three shells (b values = 1000, 2000, and 3000 s/mm^2), and 90 unique diffusion directions per shell plus 6 b = 0 s/mm^2 volumes, acquired twice with opposing phase encoding polarities. Data correspond to total scan time per subject of approximately 55 minutes. For this study, we randomly drew 50 HCP subjects (age range, 22-36 years of age, 24/26 females/males.

To assess robustness against data quality, we also used data from the UK Biobank (3T Prisma, 32 channel coil, 2 mm isotropic resolution, b values = 1000 and 2000 s/mm^2, 50 directions per shell). The UK Biobank data are acquired with approximately 6.5 minutes scan time per subject and therefore represent more standard quality datasets, achievable in a clinical scanner (*58*). Fifty subjects were randomly drawn from the UK Biobank (UKB) (age range 42-65 years of age, 31/19 females/males). For both HCP and UKB cohorts we ensured that the distribution of QC metrics (such as subject motion and image SNR/CNR) was representative of the full HCP and UKB cohorts that we had available.

4.2.3 *Macaque tracer data*

Tracer data were used to test aspects of the striatal bundle protocols (Figure 3). These were made available by SRH and were obtained from an existing collection of injections in 19 macaque brains, from (*102, 103, 104, 105, 106, 62, 107, 48, 108, 50, 109*) and cases from the laboratory of SRH. Specifically, anterograde tracers were injected across 78 cortical locations and their terminations within the putamen were recorded in coronal slices of the NMT template space at 0.5 mm resolution. Specifically, the injection sites were first assigned to one of four cortical ROIs (frontal, parietal, temporal and sensorimotor cortices), obtained from the NMT CHARM v1 parcellation (*54*). For each of these four injection ROIs, we counted all the corresponding terminations within the putamen, and then divided by the total number of termination sites. This resulted in a termination probability map for each cortical region across the putamen, and these termination maps were smoothed using spline interpolation. The putamen mask was obtained from the NMT SARM v1 parcellation (*110*). To compare against tractography in F99 space, these maps were non-linearly registered from NMT to F99 space using RheMAP (*111*).

4.3 MRI data preprocessing

4.3.1 *Crossing fibre modelling and tractography*

For both the human and macaque data, we modelled fibre orientations for up to three orientations per voxel using FSL's BEDPOSTX (*112, 113*). These orientations were used in tractography. Probabilistic tractography was performed using FSL's XTRACT (*31*), which uses FSL's PROBTRACKX (*114, 115*). The standard space protocol masks were used to seed and guide tractography, which occurred in diffusion space for each dataset. 60 major white matter fibre bundles were reconstructed (30 cortico-cortical, 29 cortico-subcortical, 1 cerebellar, Supplementary Table S1). A curvature threshold of 80° was used, the maximum number of streamline steps was 2000, and subsidiary fibres were considered above a volume fraction threshold of 1%. A step size of 0.5 mm was used for the human brain, and a step size of 0.2 mm was used for the macaque brain. Resultant spatial path distributions were normalised by the total number of valid streamlines.

4.3.2 *Registration to standard space*

For the human data, nonlinear transformations of T1-weighted (T1w) to MNI152 standard space were obtained. The distortion-corrected dMRI data were separately linearly aligned to the T1w space, and the concatenation of the diffusion-to-T1w and T1w-to-MNI transforms allowed diffusion-to-MNI warp fields to be obtained. For the macaque, nonlinear transformations to the macaque F99 standard space were estimated using FSL's FNIRT (*116*) based on the corresponding FA maps.

For cases where NMT-space tractography protocols were used, nonlinear transformations to NMT space were obtained using RheMAP (*111*).

4.4 Tractography against data quality and individual variability

4.4.1 *Varying data quality*

To explore robustness against varying data quality, we compared tractography reconstructions for in-vivo human dMRI data of considerably different data resolutions, diffusion contrast and scan time. Specifically, we explored whether tract reconstructions in state-of-the-art HCP data (approximately 55 minutes of scan time) were similar to reconstructions in bog standard data from the UK Biobank (UKB) (approximately 6.5 minutes of scan time), both on group average maps, as well as individual reconstructions.

Inter-subject variability for each tract reconstruction was assessed within and across the HCP and UKB cohorts. Inter-subject Pearson's correlations were obtained by cross correlating random subject pairs tract-wise. Specifically, for each subject pair, we correlated the normalised path distributions in MNI space for each tract, after thresholding the path distribution at 0.5% (*31*), and then averaged the correlation across tracts for each subject pair. This was repeated for all possible unique subject pairs within and across cohorts.

A pairwise Mann-Whitney U-test was performed to determine differences in variability across analyses. For example we compared the HCP vs UKB correlation between original and the new(+revised) tracts. We corrected for multiple comparisons using Bonferroni correction.

We also explored tract reconstructions on individual subjects. To demonstrate representative results, we ranked subjects based on their tractography results against the cohort average and picked the the 10th, 50th (median) and 90th percentile of the subjects. Specifically, for each subject, we calculated the average Pearson's correlation value, to the group average, across all tracts. We then ranked the subjects based on this value.

4.4.2 *Respecting similarities stemming from twinship*

As an indirect way to explore whether the proposed standardised protocols respected individual variability, we tested whether tractography reconstructions reflected similarities stemming from twinship. We used the family structure in the HCP cohort, to explore whether tracts of monozygotic twin pairs were more similar compared to tract similarity in dizygotic twins and non-twin sibling pairs, and to tract similarity in unrelated subject pairs, as would be expected by heritability of structural connections (*59,117,60*). We used the 72 pairs of monozygotic twins (MZ) available in the HCP cohort, and randomly selected 72 pairs of dizygotic twins (DZ), 72 pairs of non-twin siblings

and 72 pairs of unrelated subjects, to have a balanced comparison. We compared tracts across pairs to assess whether our automated protocols respect the underlying tract variability across individuals. Specifically, for a given subject pair and a given tract, we calculated the Pearson's correlation between the normalised path distributions (in MNI space and following thresholding at 0.5%). We repeated for all tracts and then calculated the mean correlation and standard deviation across tracts for that subject pair. This was then repeated for each group of subject pairs giving a distribution of average correlations for each group. We subsequently compared these distributions between the different groups. We repeated this process separately for the Original XTRACT tracts (*31*) and the new cortico-subcortical tracts to ensure that patterns were similar. For each analysis, a pairwise Mann-Whitney U-test was performed for all cohort pairs to determine the significant differences between them. We corrected for multiple comparisons using Bonferroni.

4.5 Building connectivity blueprints in cortex and subcortex

Connectivity blueprints are $GM \times Tracts$ matrices that have been proposed to represent the pattern of connections of GM areas to a predefined set of WM tracts (*35, 36*). To do so, the intersection of the core of WM tracts with the WM-GM boundary needs to be identified. For cortical GM, simply obtaining the intersection from the spatial path distribution maps of each tract would be dominated by the gyral bias in tractography near the cortex (*118*). Instead, whole-brain tractography matrices can be used as intermediaries. Specifically a $GM \times WM$ connectivity matrix can be generated by seeding from each location of the white-grey matter boundary and targetting to a whole WM mask and this can then be multiplied by a $WM \times Tracts$ obtained by collating the path distributions of all tracts of interest.

The cortical blueprints $GM_{ctx} \times Tracts$ were generated using our previously developed tool `xtract_blueprint` (*35, 38*). We used the GM-WM boundary surface, extracted using the HCP pipelines (*101*) for the human data and the approach in (*35*) for the macaque. Briefly, a single set of macaque surfaces were derived using a set of high-quality structural data from one of the macaque subjects. The remaining macaque data were then nonlinearly transformed to this space, and the surfaces were nonlinearly transformed to the F99 standard space. All surface data were downsampled to 10,000 vertices prior to tractography. Volume space white matter targets were downsampled to 3 mm isotropic for the human and 2 mm isotropic for the macaque.

We extended the blueprint generation to include the subcortex. For subcortical nuclei we found that using an intermediary $GM \times WM$ matrix did not help (as gyral bias is not relevant in subcortex - in fact it made patterns less specific). Hence, subcortical $GM_{sub} \times Tracts$ blueprints were built using the intersection of the path distribution of each tract with the subcortical structures of interest (i.e. through multiplication of white matter tracts and binary subcortical masks, including putamen,

caudate, thalamus, hippocampus, amygdala). Figure 9) shows a comparison of the two approaches for various tracts in the human and macaque: i) using an intermediary $GM \times WM$ matrix to obtain subcortical connection patterns, as done in (*35*) for cortical regions and ii) using directly the tractography path distributions. The latter approach gave more focal and specific patterns and was used here for the subcortical regions. Tracts were downsampled (at 2 mm for human and 1 mm for macaque), thresholded at 0.1%, and multiplied by the subcortical nuclei masks, and then vectorised and stacked to create a $GM_{sub} \times Tracts$ matrix. These were then row-wise concatenated (i.e vertically) with the cortical blueprints to generate CIFTI-style blueprints with approximately 10,000 cortical vertices and approximately 5,000 subcortical voxels (per left/right hemisphere). Finally, connectivity blueprints were row-wise sum-normalised. Following subject-wise construction of connectivity blueprints, we derived group-averaged blueprints for macaques and humans.

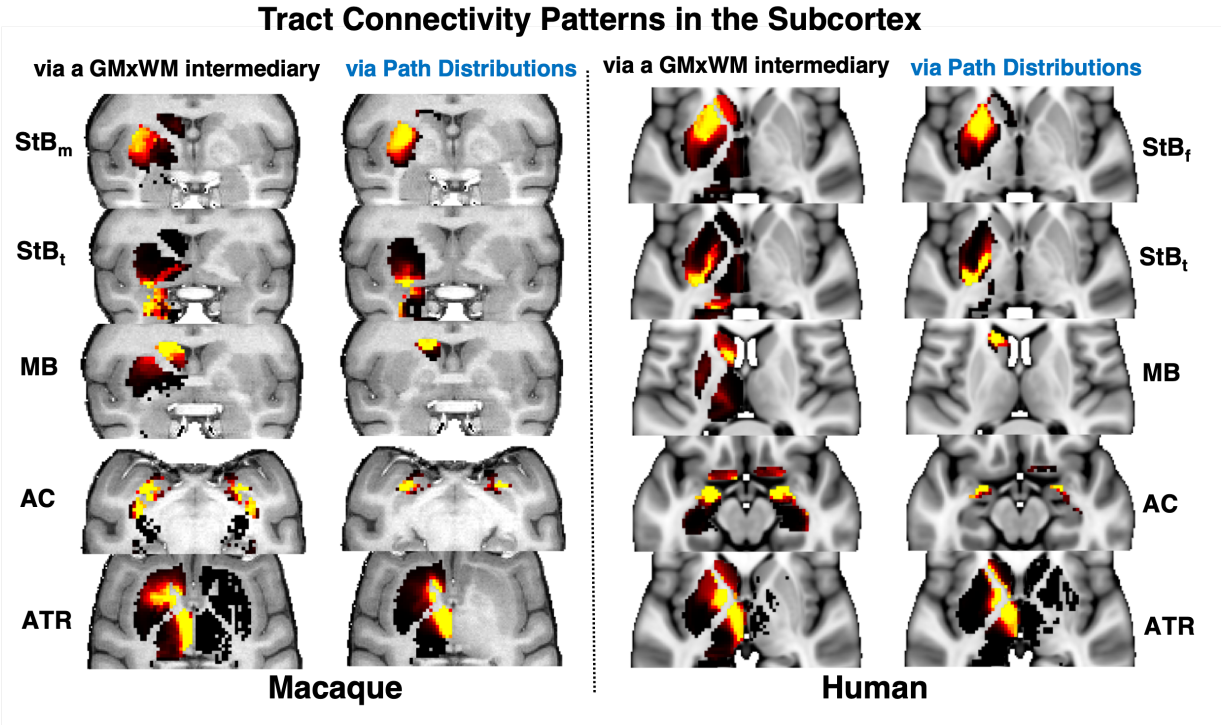

***Figure 9**: **Improved specificity in subcortical connectivity patterns when using directly the tractography path distributions.** Subcortical $GM_{sub} \times Tracts$ blueprints were built using: i) an intermediary whole brain tractography $GM \times WM$ matrix, multiplied by $WM \times Tracts$ as done in (35) for cortical regions, ii) the intersection of the path distribution of each tract with the subcortical structures of interest. The two approaches are shown on the left and right columns for each of the macaque and human examples and for representative example tracts (rows). The latter approach resulted in improved specificity in both the macaque and human, with the tract of interest connecting more focally to the relevant subcortical nucleus. For instance StB tracts end up more specifically in the putamen, MB in the caudate, AC in the amygdala and ATR in the thalamus. All examples are shown as axial views, apart from StB_m, StB_t, MB in the macaque that are shown in coronal views.*

4.6 Comparing connectivity blueprints across species

We compared grey matter connectivity patterns between humans and macaques (i.e. rows of the corresponding connectivity blueprint matrices), both in cortex and subcortex. As connectivity patterns are anchored by sets of homologously defined white matter landmarks, connectivity patterns may be compared statistically using Kullback-Leibler (KL) divergence (Equation 1) (*119*), as previously used (*35*).

Let M be the macaque connectivity blueprint matrix, with M_{ik} linking grey matter (cortex or subcortex) location i to tract $k = 1 : T$, with the set of tracts with length T. Let matrix H be the equivalent matrix for the human brain. Vertices i and j in the macaque and human brains can then be compared in terms of their connectivity patterns M_{ik}, H_{jk}, $k = 1 : T$ using the symmetric KL divergence D_{ij} as a dissimilarity measure. To avoid degeneracies in KL divergence calculations induced by the presence of zeros, we shifted all blueprint values by $\delta = 10^{-6}$. We used the tool `xtract_divergence` to perform all relevant calculations.

$$D_{ij} = \sum_k M_{ik} \log_2 \frac{M_{ik}}{H_{jk}} + \sum_k H_{jk} \log_2 \frac{H_{jk}}{M_{ik}} \tag{1}$$

Acknowledgments

Funding: SA, SW and SNS acknowledge funding from the European Research Council (ERC Consolidator — 101000969 to SNS). SNS, SJ and SH acknowledge support from the Centre for Mesoscale Connectomics (NIH UM1NS132207). The Centre for Integrative Neuroimaging was supported by the Wellcome Trust [203139/Z/16/Z]. RBM acknowledges funding from the Medical Research Council UK [MR/Y010698/1].

Author contributions: All authors contributed significantly to this work from different and, in cases, overlapping roles. The specific contributions of each are: SA: Conceptualisation, Methodology, Data Curation, Formal Analysis, Investigation, Visualisation, Writing – Original Draft, Writing – Review and Editing SW: Methodology, Data Curation, Investigation, Writing – Review and Editing DF: Methodology, Formal Analysis, Writing - Review and Editing KB: Resources, Methodology, Writing - Review and Editing AMK: Resources, Methodology WT: Resources, Methodology, Writing - Review and Editing SJ: Methodology, Resources, Writing – Review and Editing SH: Resources, Methodology, Writing – Review and Editing RM: Methodology, Formal Analysis, Writing – Review and Editing SNS: Conceptualisation, Methodology, Formal Analysis, Resources, Writing – Original Draft, Writing – Review and Editing, Supervision, Funding Acquisition

Competing interests: There are no competing interests to declare.

Data and materials availability

Human in-vivo diffusion MRI data are publicly available (www.humanconnectome.org/) and provided by the Human Connectome Project (HCP), WU-Minn Consortium (Principal Investigators: David Van Essen and Kamil Ugurbil; 1U54MH091657) funded by the 16 NIH Institutes and Centres that support the NIH Blueprint for Neuroscience Research; and by the McDonnell Centre for Systems Neuroscience at Washington University (*57*). The UK Biobank data were used under UK Biobank Project 43822 (PI: Sotiropoulos). Macaque data are openly available (https://fcon_1000.projects.nitrc.org/indi/PRIME/oxford2.html) and provided via the PRIMatE Data Exchange (http://fcon_1000.projects.nitrc.org/indi/PRIME/oxford2.html) (*100*).

Tractography protocols (https://github.com/SPMIC-UoN/xtract_data) and white matter tract atlases (https://github.com/SPMIC-UoN/XTRACT_atlases) will be made available on GitHub and will be released in FSL. Tools for performing standardised and automated tractography (XTRACT), building connectivity blueprints (xtract_blueprint) and performing divergence-based comparisons of connectivity blueprints (xtract_divergence) are available on GitHub (https://github.com/SPMIC-UoN/xtract) and are released in FSL (v6.0.7.10 onwards, https://fsl.fmrib.ox.ac.uk/fsl/docs/#/diffusion/xtract).

References

1. R. E. Passingham, K. E. Stephan, R. Kötter, The anatomical basis of functional localization in the cortex. *Nature reviews. Neuroscience* **3** (8), 606–616 (2002), doi:10.1038/nrn893.

2. R. B. Mars, R. E. Passingham, S. Jbabdi, Connectivity Fingerprints: From Areal Descriptions to Abstract Spaces. *Trends in Cognitive Sciences* **22** (11), 1026–1037 (2018), doi:https://doi.org/10.1016/j.tics.2018.08.009.

3. M. T. de Schotten, S. J. Forkel, The emergent properties of the connected brain. *Science* **378** (6619), 505–510 (2022), doi:10.1126/science.abq2591, `https://www.science.org/doi/abs/10.1126/science.abq2591`.

4. L. Pessoa, The Entangled Brain. *Journal of Cognitive Neuroscience* **35** (3), 349–360 (2023), doi:10.1162/jocn_a_01908, `https://direct.mit.edu/jocn/article/35/3/349/112783/The-Entangled-Brain`.

5. A. A. Utter, M. A. Basso, The basal ganglia: An overview of circuits and function. *Neuroscience & Biobehavioral Reviews* **32** (3), 333–342 (2008), doi:10.1016/j.neubiorev.2006.11.003, `https://linkinghub.elsevier.com/retrieve/pii/S014976340600131X`.

6. K. C. Bickart, C. I. Wright, R. J. Dautoff, B. C. Dickerson, L. F. Barrett, Amygdala volume and social network size in humans. *Nature Neuroscience* **14** (2), 163–164 (2011), doi:10.1038/nn.2724, `https://www.nature.com/articles/nn.2724`.

7. K. Berridge, M. Kringelbach, Pleasure Systems in the Brain. *Neuron* **86** (3), 646–664 (2015), doi:10.1016/j.neuron.2015.02.018, `https://linkinghub.elsevier.com/retrieve/pii/S0896627315001336`.

8. S. N. Haber, Corticostriatal circuitry. *Dialogues in Clinical Neuroscience* **18** (1), 7–21 (2016), doi:10.31887/DCNS.2016.18.1/shaber, `https://www.tandfonline.com/doi/full/10.31887/DCNS.2016.18.1/shaber`.

9. F. Z. E. Y. J. H. M. J. T. S. A. C. M. P. R. B. O. S. Evgeny J. Chumin, Joshua Faskowitz, Cortico-subcortical interactions in overlapping communities of edge functional connectivity. *Neuroimage* (2022), doi:10.1016/j.neuroimage.2022.118971.

10. D. N. Bullock, *et al.*, A taxonomy of the brain's white matter: twenty-one major tracts for the 21st century. *Cerebral Cortex (New York, N.Y.: 1991)* **32** (20), 4524–4548 (2022), doi:10.1093/cercor/bhab500.

11. M. X. Cohen, J.-C. Schoene-Bake, C. E. Elger, B. Weber, Connectivity-based segregation of the human striatum predicts personality characteristics. *Nature Neuroscience* **12** (1), 32–34 (2009), doi:10.1038/nn.2228, https://www.nature.com/articles/nn.2228.

12. B. U. Forstmann, *et al.*, Cortico-striatal connections predict control over speed and accuracy in perceptual decision making. *Proceedings of the National Academy of Sciences* **107** (36), 15916–15920 (2010), doi:10.1073/pnas.1004932107, https://pnas.org/doi/full/10.1073/pnas.1004932107.

13. S. J. Forkel, P. Friedrich, M. Thiebaut De Schotten, H. Howells, White matter variability, cognition, and disorders: a systematic review. *Brain Structure and Function* **227** (2), 529–544 (2022), doi:10.1007/s00429-021-02382-w, https://link.springer.com/10.1007/s00429-021-02382-w.

14. S. Haber, T. Behrens, The Neural Network Underlying Incentive-Based Learning: Implications for Interpreting Circuit Disruptions in Psychiatric Disorders. *Neuron* **83** (5), 1019–1039 (2014), doi:10.1016/j.neuron.2014.08.031, https://linkinghub.elsevier.com/retrieve/pii/S0896627314007326.

15. A. S. Heller, Cortical-Subcortical Interactions in Depression: From Animal Models to Human Psychopathology. *Front Syst Neurosci* (2016), doi:10.3389/fnsys.2016.00020, https://www.frontiersin.org/journals/systems-neuroscience/articles/10.3389/fnsys.2016.00020/full.

16. S. N. Haber, J. Lehman, C. Maffei, A. Yendiki, The Rostral Zona Incerta: A Subcortical Integrative Hub and Potential Deep Brain Stimulation Target for Obsessive-Compulsive Disorder. *Biological Psychiatry* **93** (11), 1010–1022 (2023), doi:10.1016/j.biopsych.2023.01.006, https://linkinghub.elsevier.com/retrieve/pii/S0006322323000100.

17. A. Weerasekera, A. Ion-Mărgineanu, G. P. Nolan, M. Mody, Subcortical-cortical white matter connectivity in adults with autism spectrum disorder and schizophrenia patients. *Psychiatry Res Neuroimaging* (2024).

18. H. Akram, *et al.*, Subthalamic deep brain stimulation sweet spots and hyperdirect cortical connectivity in Parkinson's disease. *NeuroImage* **158**, 332–345 (2017), doi:10.1016/j.neuroimage.2017.07.012, https://linkinghub.elsevier.com/retrieve/pii/S1053811917305803.

19. S. R. Heilbronner, M. V. Chafee, Learning How Neurons Fail Inside of Networks: Nonhuman Primates Provide Critical Data for Psychiatry. *Neuron* **102** (1),

21–26 (2019), doi:10.1016/j.neuron.2019.02.030, https://linkinghub.elsevier.com/retrieve/pii/S0896627319301655.

20. J. F. Lehman, B. D. Greenberg, C. C. McIntyre, S. A. Rasmussen, S. N. Haber, Rules Ventral Prefrontal Cortical Axons Use to Reach Their Targets: Implications for Diffusion Tensor Imaging Tractography and Deep Brain Stimulation for Psychiatric Illness. *Journal of Neuroscience* **31** (28), 10392–10402 (2011), publisher: Society for Neuroscience Section: Articles, doi:10.1523/JNEUROSCI.0595-11.2011, https://www.jneurosci.org/content/31/28/10392.

21. S. R. Heilbronner, S. N. Haber, Frontal Cortical and Subcortical Projections Provide a Basis for Segmenting the Cingulum Bundle: Implications for Neuroimaging and Psychiatric Disorders. *Journal of Neuroscience* **34** (30), 10041–10054 (2014), doi:10.1523/JNEUROSCI.5459-13.2014, https://www.jneurosci.org/lookup/doi/10.1523/JNEUROSCI.5459-13.2014.

22. Z. Safadi, *et al.*, Functional Segmentation of the Anterior Limb of the Internal Capsule: Linking White Matter Abnormalities to Specific Connections. *The Journal of Neuroscience* **38** (8), 2106–2117 (2018), doi:10.1523/JNEUROSCI.2335-17.2017, https://www.jneurosci.org/lookup/doi/10.1523/JNEUROSCI.2335-17.2017.

23. J. A. Oler, *et al.*, Connectivity between the central nucleus of the amygdala and the bed nucleus of the stria terminalis in the non-human primate: neuronal tract tracing and developmental neuroimaging studies. *Brain Structure and Function* **222** (1), 21–39 (2017), doi:10.1007/s00429-016-1198-9, http://link.springer.com/10.1007/s00429-016-1198-9.

24. K. Yoshida, L. Benevento, The projection from the dorsal lateral geniculate nucleus of the thalamus to extrastriate visual association cortex in the macaque monkey. *Neuroscience Letters* **22** (2), 103–108 (1981), doi:10.1016/0304-3940(81)90071-9, https://linkinghub.elsevier.com/retrieve/pii/0304394081900719.

25. S. Jbabdi, J. F. Lehman, S. N. Haber, T. E. Behrens, Human and Monkey Ventral Prefrontal Fibers Use the Same Organizational Principles to Reach Their Targets: Tracing versus Tractography. *Journal of Neuroscience* (2013).

26. D. Folloni, *et al.*, Dichotomous organization of amygdala/temporal-prefrontal bundles in both humans and monkeys. *eLife* **8** (2019), publisher: eLife Sciences Publications Ltd, doi:10.7554/ELIFE.47175.

27. S. Jbabdi, S. N. Sotiropoulos, S. N. Haber, D. C. Van Essen, T. E. Behrens, Measuring macroscopic brain connections in vivo. *Nature Neuroscience* **18** (11), 1546–1555 (2015), doi:10.1038/nn.4134.

28. S. N. Sotiropoulos, *et al.*, Advances in diffusion MRI acquisition and processing in the Human Connectome Project. *NeuroImage* **80**, 125–143 (2013), iSBN: 1053-8119 _eprint: NIHMS150003, doi:10.1016/j.neuroimage.2013.05.057.

29. S. Assimopoulos, *et al.*, Generalising XTRACT tractography protocols across common macaque brain templates. *Brain Structure and Function* (2024), doi:10.1007/s00429-024-02760-0, `https://doi.org/10.1007/s00429-024-02760-0`.

30. H. S. F. S. Sotiropoulos SN, Thiebaut de Schotten M, Cross-Species Neuroanatomy in Primates Using Tractography. *Brain Structure and Function* (2025).

31. S. Warrington, *et al.*, XTRACT - Standardised protocols for automated tractography in the human and macaque brain. *NeuroImage* **217**, 116923 (2020), doi:10.1016/j.neuroimage.2020.116923, `https://www.sciencedirect.com/science/article/pii/S1053811920304092`.

32. L. Roumazeilles, *et al.*, Longitudinal connections and the organization of the temporal cortex in macaques, great apes, and humans. *PLoS Biology* (2020).

33. K. L. Bryant, L. Li, N. Eichert, R. B. Mars, A comprehensive atlas of white matter tracts in the chimpanzee. *PLOS Biology* **18** (12), e3000971 (2020), publisher: Public Library of Science, doi:10.1371/journal.pbio.3000971, `https://journals.plos.org/plosbiology/article?id=10.1371/journal.pbio.3000971`.

34. K. L. Bryant, *et al.*, Diffusion MRI data, sulcal anatomy, and tractography for eight species from the Primate Brain Bank. *Brain Structure and Function* **226** (8), 2497–2509 (2021), doi:10.1007/s00429-021-02268-x, `https://doi.org/10.1007/s00429-021-02268-x`.

35. R. B. Mars, *et al.*, Whole brain comparative anatomy using connectivity blueprints. *eLife* **7** (e35237) (2018), publisher: Cold Spring Harbor Laboratory, doi:10.7554/eLife.35237.

36. R. B. Mars, S. Jbabdi, M. F. S. Rushworth, A Common Space Approach to Comparative Neuroscience. *Annual review of neuroscience* **44**, 69–86 (2021), doi:10.1146/annurev-neuro-100220-025942.

37. M. Thiebaut De Schotten, C. Foulon, P. Nachev, Brain disconnections link structural connectivity with function and behaviour. *Nature Communications* **11** (1), 5094 (2020), doi:10.1038/s41467-020-18920-9, https://www.nature.com/articles/s41467-020-18920-9.

38. S. Warrington, *et al.*, Concurrent mapping of brain ontogeny and phylogeny within a common space: Standardized tractography and applications. *Science Advances* **8** (42), eabq2022 (2022), publisher: American Association for the Advancement of Science, doi:10.1126/sciadv.abq2022, https://www.science.org/doi/10.1126/sciadv.abq2022.

39. D. Wassermann, *et al.*, The white matter query language: a novel approach for describing human white matter anatomy. *Brain Structure and Function* **221** (9), 4705–4721 (2016), doi:10.1007/s00429-015-1179-4, http://link.springer.com/10.1007/s00429-015-1179-4.

40. J. Wasserthal, P. Neher, K. H. Maier-Hein, TractSeg - Fast and accurate white matter tract segmentation. *NeuroImage* **183**, 239–253 (2018), doi:10.1016/j.neuroimage.2018.07.070, https://linkinghub.elsevier.com/retrieve/pii/S1053811918306864.

41. C. Maffei, *et al.*, Using diffusion MRI data acquired with ultra-high gradient strength to improve tractography in routine-quality data. *NeuroImage* **245**, 118706 (2021), doi:10.1016/j.neuroimage.2021.118706, https://linkinghub.elsevier.com/retrieve/pii/S1053811921009782.

42. S. J. Forkel, *et al.*, The anatomy of fronto-occipital connections from early blunt dissections to contemporary tractography. *Cortex* **56**, 73–84 (2014), doi:10.1016/j.cortex.2012.09.005, https://linkinghub.elsevier.com/retrieve/pii/S0010945212002882.

43. K. G. Schilling, *et al.*, Brain connections derived from diffusion MRI tractography can be highly anatomically accurate—if we know where white matter pathways start, where they end, and where they do not go. *Brain Structure and Function* **225** (8), 2387–2402 (2020), doi:10.1007/s00429-020-02129-z, https://link.springer.com/10.1007/s00429-020-02129-z.

44. R. B. Mars, *et al.*, The extreme capsule fiber complex in humans and macaque monkeys: a comparative diffusion MRI tractography study. *Brain Structure and Function* **221** (8), 4059–4071 (2016), publisher: Springer, doi:10.1007/s00429-015-1146-0.

45. D. C. Van Essen, Windows on the brain: The emerging role of atlases and databases in neuroscience. *Current Opinion in Neurobiology* **12** (5), 574–579 (2002), doi:10.1016/S0959-4388(02)00361-6.

46. M. F. Glasser, D. C. Van Essen, Mapping Human Cortical Areas *In Vivo* Based on Myelin Content as Revealed by T1- and T2-Weighted MRI. *The Journal of Neuroscience* **31** (32), 11597–11616 (2011), doi:10.1523/JNEUROSCI.2180-11.2011, https://www.jneurosci.org/lookup/doi/10.1523/JNEUROSCI.2180-11.2011.

47. J. Seidlitz, *et al.*, A population MRI brain template and analysis tools for the macaque. *NeuroImage* **170**, 121–131 (2018), doi:10.1016/j.neuroimage.2017.04.063, https://linkinghub.elsevier.com/retrieve/pii/S105381191730383X.

48. J. D. Schmahmann, D. N. Pandya, *Fiber Pathways of the Brain* (2006), doi:10.1093/acprof:oso/9780195104233.001.0001, publication Title: Fiber Pathways of the Brain.

49. N. Makris, D. N. Pandya, The extreme capsule in humans and rethinking of the language circuitry. *Brain Structure and Function* **213** (3), 343–358 (2009), doi:10.1007/s00429-008-0199-8, http://link.springer.com/10.1007/s00429-008-0199-8.

50. E. Y. Choi, S.-L. Ding, S. N. Haber, Combinatorial Inputs to the Ventral Striatum from the Temporal Cortex, Frontal Cortex, and Amygdala: Implications for Segmenting the Striatum. *eneuro* **4** (6), ENEURO.0392–17.2017 (2017), doi:10.1523/ENEURO.0392-17.2017, https://www.eneuro.org/lookup/doi/10.1523/ENEURO.0392-17.2017.

51. C. Liu, *et al.*, A resource for the detailed 3D mapping of white matter pathways in the marmoset brain. *Nature Neuroscience* **23** (2), 271–280 (2020), publisher: Nature Publishing Group, doi:10.1038/s41593-019-0575-0, https://www.nature.com/articles/s41593-019-0575-0.

52. M. Petrides, D. Pandya, Efferent association pathways originating in the caudal prefrontal cortex in the macaque monkey. *The Journal of Comparative Neurology* **498** (2), 227–251 (2006), doi:10.1002/cne.21048, https://onlinelibrary.wiley.com/doi/10.1002/cne.21048.

53. J. A. Oler, J. L. Fudge, Prefrontal Cortex: A tale of two pathways. *eLife* **8**, e51990 (2019), doi:10.7554/eLife.51990, https://doi.org/10.7554/eLife.51990.

54. B. Jung, *et al.*, A comprehensive macaque fMRI pipeline and hierarchical atlas. *NeuroImage* **235**, 117997 (2021), doi:10.1016/j.neuroimage.2021.117997, https://www.sciencedirect.com/science/article/pii/S1053811921002743.

55. J. A. Frazier, *et al.*, Structural Brain Magnetic Resonance Imaging of Limbic and Thalamic Volumes in Pediatric Bipolar Disorder. *American Journal of Psychiatry* **162** (7), 1256–

1265 (2005), publisher: American Psychiatric Publishing, doi:10.1176/appi.ajp.162.7.1256, https://psychiatryonline.org/doi/10.1176/appi.ajp.162.7.1256.

56. R. S. Desikan, *et al.*, An automated labeling system for subdividing the human cerebral cortex on MRI scans into gyral based regions of interest. *NeuroImage* (2006), doi:10.1016/j.neuroimage.2006.01.021.

57. D. C. Van Essen, *et al.*, The WU-Minn Human Connectome Project: an overview. *NeuroImage* **80**, 62–79 (2013), doi:10.1016/j.neuroimage.2013.05.041, http://linkinghub.elsevier.com/retrieve/pii/S1053811913005351%5Cnpapers3://publication/doi/10.1016/j.neuroimage.2013.05.041.

58. K. L. Miller, *et al.*, Multimodal population brain imaging in the UK Biobank prospective epidemiological study. *Nature Neuroscience* **19** (11), 1523–1536 (2016), doi:10.1038/nn.4393, https://www.nature.com/articles/nn.4393.

59. M. M. Bohlken, *et al.*, Heritability of structural brain network topology: A DTI study of 156 twins. *Human Brain Mapping* **35** (10), 5295–5305 (2014), doi:10.1002/hbm.22550, https://onlinelibrary.wiley.com/doi/10.1002/hbm.22550.

60. K.-K. Shen, *et al.*, Investigating brain connectivity heritability in a twin study using diffusion imaging data. *NeuroImage* **100**, 628–641 (2014), doi:10.1016/j.neuroimage.2014.06.041, https://linkinghub.elsevier.com/retrieve/pii/S1053811914005187.

61. T. B. Yeo, *et al.*, The organization of the human cerebral cortex estimated by intrinsicfunctional connectivity. *Journal of Neurophysiology* **106** (3), 1125–1165 (2011), publisher: Society for Neuroscience Section: Articles, doi:10.1152/jn.00338.2011, https://journals.physiology.org/doi/epdf/10.1152/jn.00338.2011.

62. S. N. Haber, K.-S. Kim, P. Mailly, R. Calzavara, Reward-Related Cortical Inputs Define a Large Striatal Region in Primates That Interface with Associative Cortical Connections, Providing a Substrate for Incentive-Based Learning. *The Journal of Neuroscience* **26** (32), 8368–8376 (2006), doi:10.1523/JNEUROSCI.0271-06.2006, https://www.jneurosci.org/lookup/doi/10.1523/JNEUROSCI.0271-06.2006.

63. S. Oldham, G. Ball, A phylogenetically-conserved axis of thalamocortical connectivity in the human brain. *Nature Communications* **14** (1), 6032 (2023), doi:10.1038/s41467-023-41722-8, https://www.nature.com/articles/s41467-023-41722-8.

64. C. M. A. Pennartz, *et al.*, Corticostriatal Interactions during Learning, Memory Processing, and Decision Making. *The Journal of Neuroscience* **29** (41), 12831–12838 (2009), doi:10.1523/JNEUROSCI.3177-09.2009, https://www.jneurosci.org/lookup/doi/10.1523/JNEUROSCI.3177-09.2009.

65. S. M. Sherman, Thalamus plays a central role in ongoing cortical functioning. *nature neuroscience* **19** (4) (2016).

66. K. G. Cruz, *et al.*, Cortical-subcortical interactions in goal-directed behavior. *Physiological Reviews* **103** (1), 347–389 (2023), doi:10.1152/physrev.00048.2021, https://journals.physiology.org/doi/10.1152/physrev.00048.2021.

67. S. K. Peters, K. Dunlop, J. Downar, Cortico-Striatal-Thalamic Loop Circuits of the Salience Network: A Central Pathway in Psychiatric Disease and Treatment. *Frontiers in Systems Neuroscience* **10** (2016), doi:10.3389/fnsys.2016.00104, http://journal.frontiersin.org/article/10.3389/fnsys.2016.00104/full.

68. K. D. Bhatia, L. A. Henderson, E. Hsu, M. Yim, Reduced integrity of the uncinate fasciculus and cingulum in depression: A stem-by-stem analysis. *Journal of Affective Disorders* **235**, 220–228 (2018), doi:10.1016/j.jad.2018.04.055, https://linkinghub.elsevier.com/retrieve/pii/S0165032718303951.

69. A. F. Arnsten, K. Rubia, Neurobiological Circuits Regulating Attention, Cognitive Control, Motivation, and Emotion: Disruptions in Neurodevelopmental Psychiatric Disorders. *Journal of the American Academy of Child & Adolescent Psychiatry* **51** (4), 356–367 (2012), doi:10.1016/j.jaac.2012.01.008, https://linkinghub.elsevier.com/retrieve/pii/S0890856712000433.

70. M. Jalbrzikowski, *et al.*, Development of White Matter Microstructure and Intrinsic Functional Connectivity Between the Amygdala and Ventromedial Prefrontal Cortex: Associations With Anxiety and Depression. *Biological Psychiatry* **82** (7), 511–521 (2017), doi:10.1016/j.biopsych.2017.01.008, https://linkinghub.elsevier.com/retrieve/pii/S0006322317300409.

71. L. S. Van Velzen, *et al.*, White matter disturbances in major depressive disorder: a coordinated analysis across 20 international cohorts in the ENIGMA MDD working group. *Molecular Psychiatry* **25** (7), 1511–1525 (2020), doi:10.1038/s41380-019-0477-2, https://www.nature.com/articles/s41380-019-0477-2.

72. J. J. Levitt, *et al.*, Reduced Structural Connectivity in Frontostriatal White Matter Tracts in the Associative Loop in Schizophrenia. *American Journal of Psychiatry* **174** (11), 1102–1111 (2017), doi:10.1176/appi.ajp.2017.16091046, http://ajp.psychiatryonline.org/doi/10.1176/appi.ajp.2017.16091046.

73. N. Ikeda, *et al.*, Structural connectivity between the hippocampus and cortical/subcortical area relates to cognitive impairment in schizophrenia but not in mood disorders. *Journal of Neuropsychology* **17** (2), 351–363 (2023), doi:10.1111/jnp.12298, https://bpspsychub.onlinelibrary.wiley.com/doi/10.1111/jnp.12298.

74. R. J. Theilmann, *et al.*, White-Matter Changes Correlate with Cognitive Functioning in Parkinson's Disease. *Frontiers in Neurology* **4** (2013), doi:10.3389/fneur.2013.00037, http://journal.frontiersin.org/article/10.3389/fneur.2013.00037/abstract.

75. R. J. Von Der Heide, L. M. Skipper, E. Klobusicky, I. R. Olson, Dissecting the uncinate fasciculus: disorders, controversies and a hypothesis. *Brain* **136** (6), 1692–1707 (2013), doi:10.1093/brain/awt094, https://academic.oup.com/brain/article-lookup/doi/10.1093/brain/awt094.

76. A. R. Khan, *et al.*, Biomarkers of Parkinson's disease: Striatal sub-regional structural morphometry and diffusion MRI. *NeuroImage: Clinical* **21**, 101597 (2019), doi:10.1016/j.nicl.2018.11.007, https://linkinghub.elsevier.com/retrieve/pii/S2213158218303450.

77. S. Marecek, *et al.*, Analysis of striatal connectivity corresponding to striosomes and matrix in de novo Parkinson's disease and isolated REM behavior disorder. *npj Parkinson's Disease* **10** (1), 124 (2024), doi:10.1038/s41531-024-00736-9, https://www.nature.com/articles/s41531-024-00736-9.

78. E. J. Bubb, C. Metzler-Baddeley, J. P. Aggleton, The cingulum bundle: Anatomy, function, and dysfunction. *Neuroscience & Biobehavioral Reviews* **92**, 104–127 (2018), doi:10.1016/j.neubiorev.2018.05.008, https://linkinghub.elsevier.com/retrieve/pii/S0149763418300198.

79. M. Langen, *et al.*, Fronto-striatal circuitry and inhibitory control in autism: Findings from diffusion tensor imaging tractography. *Cortex* **48** (2), 183–193 (2012), doi:10.1016/j.cortex.2011.05.018, https://linkinghub.elsevier.com/retrieve/pii/S0010945211001626.

80. E. Kilroy, *et al.*, Specific tractography differences in autism compared to developmental coordination disorder. *Scientific Reports* **12** (1), 19246 (2022), doi:10.1038/s41598-022-21538-0, https://www.nature.com/articles/s41598-022-21538-0.

81. S. N. Haber, A. Yendiki, S. Jbabdi, Four Deep Brain Stimulation Targets for Obsessive-Compulsive Disorder: Are They Different? *Biological Psychiatry* **90** (10), 667–677 (2021), doi:10.1016/j.biopsych.2020.06.031, https://linkinghub.elsevier.com/retrieve/pii/S000632232031773X.

82. S. Alagapan, *et al.*, Cingulate dynamics track depression recovery with deep brain stimulation. *Nature* **622** (7981), 130–138 (2023), doi:10.1038/s41586-023-06541-3, https://www.nature.com/articles/s41586-023-06541-3.

83. N. Pouratian, *et al.*, Multi-institutional evaluation of deep brain stimulation targeting using probabilistic connectivity-based thalamic segmentation: Clinical article. *Journal of Neurosurgery* **115** (5), 995–1004 (2011), doi:10.3171/2011.7.JNS11250, https://thejns.org/view/journals/j-neurosurg/115/5/article-p995.xml.

84. K. Dunlop, *et al.*, Dorsomedial prefrontal cortex repetitive transcranial magnetic stimulation for treatment-refractory major depressive disorder: A three-arm, blinded, randomized controlled trial. *Brain Stimulation* **13** (2), 337–340 (2020), doi:10.1016/j.brs.2019.10.020, https://linkinghub.elsevier.com/retrieve/pii/S1935861X19304292.

85. H. Gan, *et al.*, High frequency repetitive transcranial magnetic stimulation of dorsomedial prefrontal cortex for negative symptoms in patients with schizophrenia: A double-blind, randomized controlled trial. *Psychiatry Research* **299**, 113876 (2021), doi:10.1016/j.psychres.2021.113876, https://linkinghub.elsevier.com/retrieve/pii/S0165178121001736.

86. R. Bodén, J. Bengtsson, E. Thörnblom, W. Struckmann, J. Persson, Dorsomedial prefrontal theta burst stimulation to treat anhedonia, avolition, and blunted affect in schizophrenia or depression – a randomized controlled trial. *Journal of Affective Disorders* **290**, 308–315 (2021), doi:10.1016/j.jad.2021.04.053, https://linkinghub.elsevier.com/retrieve/pii/S0165032721003852.

87. F.-j. Chen, Repetitive Transcranial Magnetic Stimulation Improves Amygdale Functional Connectivity in Major Depressive Disorder. *Frontiers in Psychiatry* **11** (2020).

88. T. Kroker, *et al.*, Noninvasive stimulation of the ventromedial prefrontal cortex modulates rationality of human decision-making. *Scientific Reports* **12** (1), 20213 (2022), doi:10.1038/s41598-022-24526-6, https://www.nature.com/articles/s41598-022-24526-6.

89. T. E. Moses, *et al.*, Left ventromedial prefrontal cortex inhibitory rTMS as an anti-stress intervention in opioid use disorder: Trial design. *Contemporary Clinical Trials Communications* **43**, 101414 (2025), doi:10.1016/j.conctc.2024.101414, https://linkinghub.elsevier.com/retrieve/pii/S2451865424001613.

90. N. L. Balderston, Mechanistic link between right prefrontal cortical activity and anxious arousal revealed using transcranial magnetic stimulation in healthy subjects (2020).

91. S. M. Fitzsimmons, E. Oostra, T. S. Postma, Y. D. Van Der Werf, O. A. Van Den Heuvel, Repetitive Transcranial Magnetic Stimulation–Induced Neuroplasticity and the Treatment of Psychiatric Disorders: State of the Evidence and Future Opportunities. *Biological Psychiatry* **95** (6), 592–600 (2024), doi:10.1016/j.biopsych.2023.11.016, https://linkinghub.elsevier.com/retrieve/pii/S0006322323017456.

92. R. L. C. Barrett, *et al.*, Differences in Frontal Network Anatomy Across Primate Species. *The Journal of Neuroscience* **40** (10), 2094–2107 (2020), doi:10.1523/JNEUROSCI.1650-18.2019, https://www.jneurosci.org/lookup/doi/10.1523/JNEUROSCI.1650-18.2019.

93. K. L. Bryant, *et al.*, Connectivity profile and function of uniquely human cortical areas. *The Journal of Neuroscience* p. e2017242025 (2025), doi:10.1523/JNEUROSCI.2017-24.2025, https://www.jneurosci.org/lookup/doi/10.1523/JNEUROSCI.2017-24.2025.

94. B. C. Tendler, *et al.*, The Digital Brain Bank, an open access platform for post-mortem imaging datasets. *eLife* **11**, e73153 (2022), doi:10.7554/eLife.73153, https://doi.org/10.7554/eLife.73153.

95. K. L. Bryant, *et al.*, A map of white matter tracts in a lesser ape, the lar gibbon. *Brain Structure and Function* (2023), doi:10.1007/s00429-023-02709-9, https://link.springer.com/10.1007/s00429-023-02709-9.

96. M. L. Jouandet, M. S. Gazzaniga, Cortical field of origin of the anterior commissure of the rhesus monkey. *Experimental Neurology* **66** (2), 381–397 (1979), doi:10.1016/0014-4886(79)90088-8, https://www.sciencedirect.com/science/article/pii/0014488679900888.

97. M. Catani, M. Thiebaut de Schotten, Atlas of Human Brain Connections (all tracts), in *Atlas of Human Brain Connections* (2013), doi:10.1093/med/9780199541164.003.0073.

98. L. R. Fenlon, R. Suarez, Z. Lynton, L. J. Richards, The evolution, formation and connectivity of the anterior commissure. *Seminars in Cell & Developmental Biology* **118**, 50–59 (2021), doi:10.1016/j.semcdb.2021.04.009, https://www.sciencedirect.com/science/article/pii/S1084952121000823.

99. R. Hartig, *et al.*, The Subcortical Atlas of the Rhesus Macaque (SARM) for neuroimaging. *NeuroImage* **235**, 117996 (2021), doi:10.1016/j.neuroimage.2021.117996, https://www.sciencedirect.com/science/article/pii/S1053811921002731.

100. M. P. Milham, *et al.*, An Open Resource for Non-human Primate Imaging. *Neuron* **100** (1), 61–74 (2018), doi:10.1016/j.neuron.2018.08.039.

101. M. F. Glasser, *et al.*, The minimal preprocessing pipelines for the Human Connectome Project. *NeuroImage* **80**, 105–124 (2013), iSBN: 1053-8119 _eprint: NIHMS150003, doi:10.1016/j.neuroimage.2013.04.127.

102. J. T. Weber, T. C. T. Yin, Subcortical projections of the inferior parietal cortex (area 7) in the stump-tailed monkey. *Journal of Comparative Neurology* **224** (2), 206–230 (1984), doi:10.1002/cne.902240204, https://onlinelibrary.wiley.com/doi/10.1002/cne.902240204.

103. J. S. Baizer, R. Desimone, L. G. Ungerleider, Comparison of subcortical connections of inferior temporal and posterior parietal cortex in monkeys. *Visual Neuroscience* **10** (1), 59–72 (1993), doi:10.1017/S0952523800003229, https://www.cambridge.org/core/product/identifier/S0952523800003229/type/journal_article.

104. E. H. Yeterian, D. N. Pandya, Corticostriatal connections of extrastriate visual areas in rhesus monkeys. *Journal of Comparative Neurology* **352** (3), 436–457 (1995), doi:10.1002/cne.903520309, https://onlinelibrary.wiley.com/doi/10.1002/cne.903520309.

105. E. Yeterian, D. Pandya, Corticostriatal connections of the superior temporal region in rhesus monkeys. *The Journal of Comparative Neurology* **399** (3), 384–402 (1998), doi:10.1002/(SICI)1096-9861(19980928)399:3⟨384::AID-CNE7⟩3.0.CO;2-X, https://onlinelibrary.wiley.com/doi/10.1002/(SICI)1096-9861(19980928)399:3<384::AID-CNE7>3.0.CO;2-X.

106. A. T. Ferry, D. NgR, X. An, J. L. Price, Prefrontal cortical projections to the striatum in macaque monkeys: Evidence for an organization related to prefrontal networks. *The Journal of Comparative Neurology* **425** (3), 447–470 (2000), doi:10.1002/1096-9861(20000925)425:

3⟨447::AID-CNE9⟩3.0.CO;2-V, https://onlinelibrary.wiley.com/doi/10.1002/1096-9861(20000925)425:3<447::AID-CNE9>3.0.CO;2-V.

107. J. Parvizi, G. W. Van Hoesen, J. Buckwalter, A. Damasio, Neural connections of the posteromedial cortex in the macaque. *Proceedings of the National Academy of Sciences* **103** (5), 1563–1568 (2006), doi:10.1073/pnas.0507729103, https://pnas.org/doi/full/10.1073/pnas.0507729103.

108. R. Calzavara, P. Mailly, S. N. Haber, Relationship between the corticostriatal terminals from areas 9 and 46, and those from area 8A, dorsal and rostral premotor cortex and area 24c: an anatomical substrate for cognition to action. *European Journal of Neuroscience* **26** (7), 2005–2024 (2007), doi:10.1111/j.1460-9568.2007.05825.x, https://onlinelibrary.wiley.com/doi/10.1111/j.1460-9568.2007.05825.x.

109. E. Y. Choi, Y. Tanimura, P. R. Vage, E. H. Yates, S. N. Haber, Convergence of prefrontal and parietal anatomical projections in a connectional hub in the striatum. *NeuroImage* **146**, 821–832 (2017), doi:10.1016/j.neuroimage.2016.09.037, https://linkinghub.elsevier.com/retrieve/pii/S1053811916305146.

110. R. Hartig, *et al.*, The Subcortical Atlas of the Rhesus Macaque (SARM) for neuroimaging. *NeuroImage* **235**, 117996 (2021), doi:https://doi.org/10.1016/j.neuroimage.2021.117996, https://www.sciencedirect.com/science/article/pii/S1053811921002731.

111. C. Klink, N. Sirmpilatze, PRIME-RE/RheMAP: RheMAP v1.3 ”Corona Edition” (2020).

112. S. Jbabdi, S. N. Sotiropoulos, A. M. Savio, M. Graña, T. E. Behrens, Model-based analysis of multishell diffusion MR data for tractography: How to get over fitting problems. *Magnetic Resonance in Medicine* **68** (6), 1846–1855 (2012), doi:10.1002/mrm.24204.

113. M. Hernández, *et al.*, Accelerating Fibre Orientation Estimation from Diffusion Weighted Magnetic Resonance Imaging Using GPUs. *PLoS ONE* **8** (4), e61892 (2013), doi:10.1371/journal.pone.0061892, https://dx.plos.org/10.1371/journal.pone.0061892.

114. T. E. J. Behrens, H. Johansen-Berg, S. Jbabdi, M. Rushworth, M. Woolrich, Probabilistic diffusion tractography with multiple fibre orientations: What can we gain? *NeuroImage* **34** (1), 144–155 (2007), iSBN: 1053-8119 (Print)\r1053-8119 (Linking), doi:10.1016/j.neuroimage.2006.09.018.

115. M. Hernandez-Fernandez, *et al.*, Using GPUs to accelerate computational diffusion MRI: From microstructure estimation to tractography and connectomes. *NeuroImage* **188**, 598–

615 (2019), doi:10.1016/j.neuroimage.2018.12.015, https://linkinghub.elsevier.com/retrieve/pii/S1053811918321591.

116. J. L. R. Andersson, M. Jenkinson, S. M. Smith, Non-linear optimisation. FMRIB technical report TR07JA1. *In prac.* (2007), iSBN: TR07JA2, doi:10.1109/EMOBILITY.2010.5668100.

117. A. G. Jansen, S. E. Mous, T. White, D. Posthuma, T. J. C. Polderman, What Twin Studies Tell Us About the Heritability of Brain Development, Morphology, and Function: A Review. *Neuropsychology Review* **25** (1), 27–46 (2015), doi:10.1007/s11065-015-9278-9, http://link.springer.com/10.1007/s11065-015-9278-9.

118. D. C. Van Essen, *et al.*, Chapter 16 - Mapping Connections in Humans and Non-Human Primates: Aspirations and Challenges for Diffusion Imaging (Academic Press, San Diego), pp. 337–358 (2014), doi:https://doi.org/10.1016/B978-0-12-396460-1.00016-0, https://www.sciencedirect.com/science/article/pii/B9780123964601000160.

119. S. Kullback, R. A. Leibler, On Information and Sufficiency. *The Annals of Mathematical Statistics* (1951), doi:10.1214/aoms/1177729694.

120. S. Wakana, H. Jiang, L. M. Nagae-Poetscher, P. C. van Zijl, S. Mori, Fiber tract-based atlas of human white matter anatomy. *Radiology* (2004), doi:10.1148/radiol.2301021640.

Supplementary Materials for Cross-species Standardised Cortico-Subcortical Tractography

Stephania Assimopoulos, Shaun Warrington, Davide Folloni, Katherine Bryant, Wei Tang, Saad Jbabdi, Sarah Heilbronner, Rogier B Mars, Stamatios N Sotiropoulos

*Corresponding author. Email: stamatios.sotiropoulos@nottingham.ac.uk

Original cortico-thalamic XTRACT protocols

For completeness of presenting all the cortico-subcortical protocols, we include here the previously published protocols of thalamic radiations (*31*).

Acoustic Radiation (AR): The acoustic radiation connects the medial geniculate nucleus (MGN) of the thalamus to the auditory cortex. The seed was placed in the transverse temporal gyrus and the target covered the MGN of the thalamus. The exclusion mask consisted of two coronal planes, anterior and posterior to the thalamus, and an axial plane superior to the thalamus. In addition, the exclusion mask contained the brainstem and a horizontal region covering the optic tract.

Anterior Thalamic Radiation (ATR): The anterior thalamic radiation connects the thalamus to the frontal lobe. The seed mask was a coronal mask through the anterior part of the thalamus (*120*), with a coronal target mask at the anterior thalamic peduncle. In addition, the exclusion mask contained an axial plane covering the base of the midbrain, a coronal plane preventing leakage via the posterior thalamic peduncle and a coronal plane preventing leakage via the cingulum. A coronal stop mask covered the posterior part of the thalamus, extending from the base of the midbrain to the callosal sulcus.

Optic Radiation (OR): The optic radiation consists of fibres from the lateral geniculate nucleus (LGN) of the thalamus to the primary visual cortex. The seed was placed in the LGN and the target mask consisted of a coronal plane through the anterior part of the calcarine fissure. Exclusion masks consisted of an axial block of the brainstem, a coronal block of fibres directly posterior to the LGN to select fibres that curl around dorsally, and a coronal plane anterior to the seed to prevent leaking into longitudinal fibres.

Superior Thalamic Radiation (STR): The superior thalamic radiation connects the thalamus to

the pre-/post-central gyrus respectively. The seed was a mask covering the whole thalamus and the target an axial plane covering the superior thalamic peduncle. An axial plane was used as a stop mask ventrally to the thalamus. The exclusion mask included two coronal planes, anterior and posterior to the target, to exclude tracking to the prefrontal cortex and occipital cortex respectively.

***Table S1**: **List of all species-matched (human & macaque) tract protocols**, grouped as cortico-cortical, cortico-subcortical and cerebellar. Columns indicate whether corresponding protocols are bilateral or not and whether they are New, Revised or not changed (Original XTRACT).*

Cortico-Cortical	**Abbreviation**	**Bilateral**	**Version**
Arcuate Fasciculus	AF	Yes	Original
Cingulum subsection : Dorsal	CBD	Yes	Original
Cingulum subsection : Peri-genual	CBP	Yes	Original
Cingulum subsection : Temporal	CBT	Yes	Original
Corticospinal Tract	CST	Yes	Original
Frontal Aslant	FA	Yes	Original
Forceps Major	FMA	No	Original
Forceps Minor	FMI	No	Original
Inferior Longitudinal Fasciculus	ILF	Yes	Original
Inferior Fronto-Occipital Fasciculus	IFO	Yes	Original
Middle Longitudinal Fasciculus	$MdLF$	Yes	Original
Superior Longitudinal Fasciculus 1	$SLF1$	Yes	Original
Superior Longitudinal Fasciculus 2	$SLF2$	Yes	Original
Superior Longitudinal Fasciculus 3	$SLF3$	Yes	Original
Vertical Occipital Fasciculus	VOF	Yes	Original
Uncinate Fasciculus	UF	Yes	Revised
Cortico-Subcortical			
Acoustic Radiation	AR	Yes	Original
Anterior Thalamic Radiation	ATR	Yes	Original
Optic Radiation	OR	Yes	Original
Superior Thalamic Radiation	STR	Yes	Original
Fornix	FX	Yes	Revised
Anterior Commissure	AC	No	Revised
Amygdalofugal Tract	AMF	Yes	New
Muratoff Bundle/Subcallosal Fasciculus	MB	Yes	New
Striatal Bundle/External Capsule (sensorimotor)	StB_m	Yes	New
Striatal Bundle/External Capsule (frontal)	StB_f	Yes	New
Striatal Bundle/External Capsule (temporal)	StB_t	Yes	New
Striatal Bundle/External Capsule (parietal)	StB_p	Yes	New
Extreme Capsule (frontal)	EmC_f	Yes	New
Extreme Capsule (temporal)	EmC_t	Yes	New
Extreme Capsule (parietal)	EmC_p	Yes	New
Cerebellar			
Middle Cerebellar Peduncle	MCP	No	Original

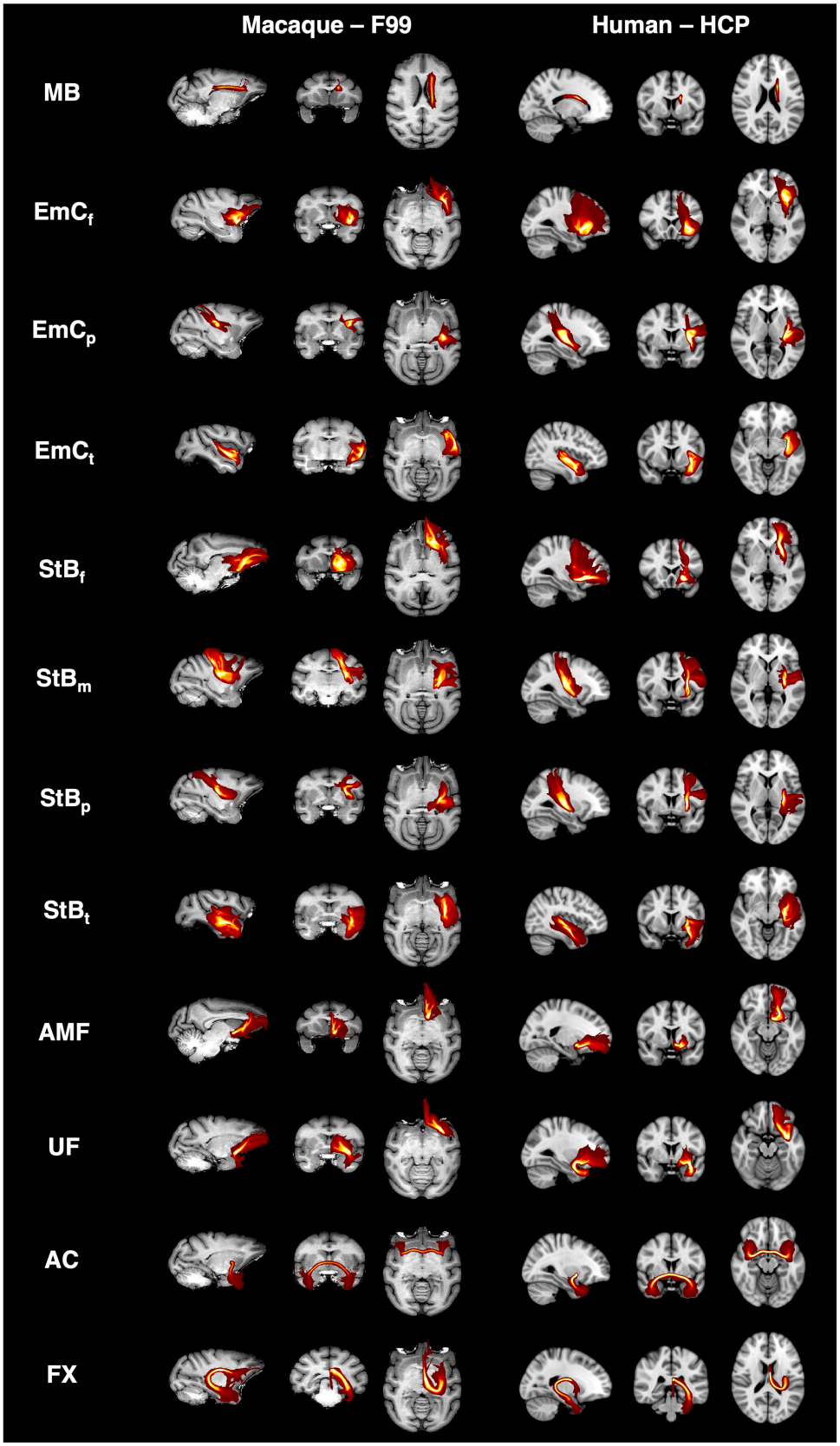

***Figure S1**: Tract reconstructions using our cortico-subcortical protocols, with good agreement between the macaque and the human.* *Maximum intensity projections (MIPs) of the group-averaged path distributions for all developed tractography protocols in the macaque (6 animal average) and human (50 healthy subject average from the Human Connectome Project dataset; HCP). All MIPs are across a window (20% of the field of view) centred at the displayed slices. Thresholded path distributions are displayed with a low threshold of 0.1% (for the EmC parts the 90th percentile was used).*

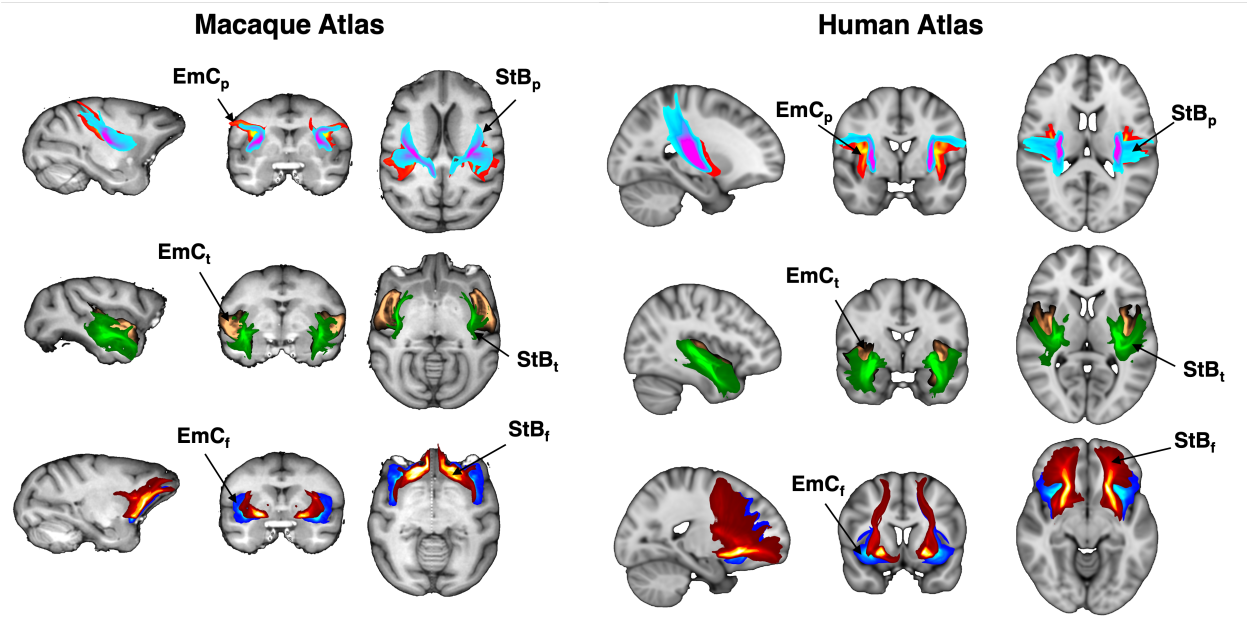

***Figure S2**: **Relative positions maintained for all corresponding parts of striatal and extreme capsule bundles, across species.** Maximum intensity projections (MIPs) of the group-averaged tractography results for corresponding parts of the striatal bundle (StB)/external capsule and the extreme capsule (EmC) in the macaque (6 animal average) and human (50 healthy subject average from the Human Connectome Project dataset; HCP). For each part, StB is more medial and EmC is more lateral (with respect to each other. Tracts considered: frontal, temporal and parietal parts of the anterior limb of the extreme capsule (EmC_f, EmC_t, EmC_p); frontal, temporal and parietal parts of the striatal bundle (StB_f, StB_t, StB_p) (Table 1 in main text).*

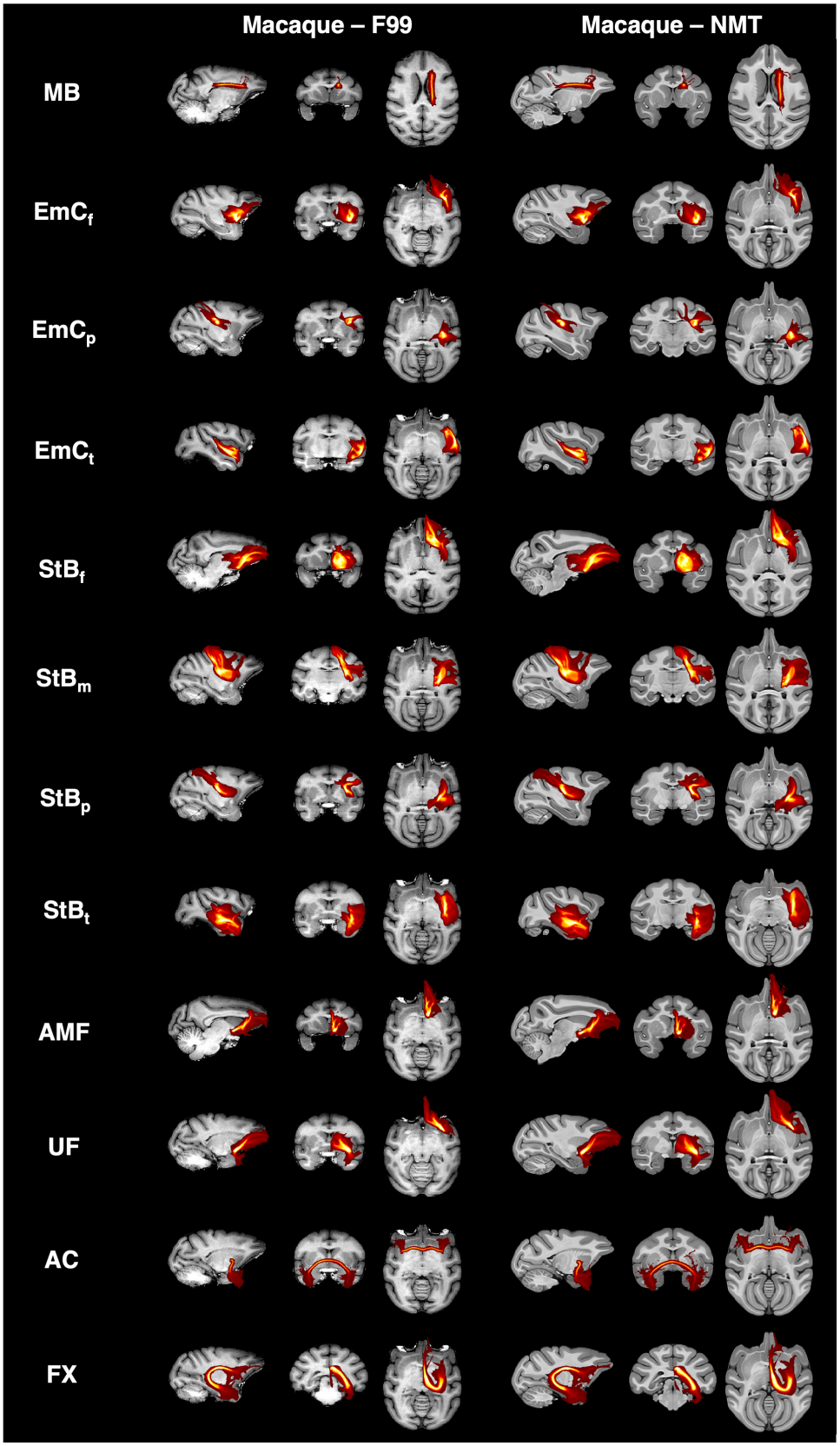

***Figure S3**: Corresponding tract reconstructions using our macaque cortico-subcortical protocols, between the two macaque standard spaces, F99 and NMT.* *Maximum intensity projections (MIPs) of the group-averaged path distributions for all developed tractography results for all developed protocols in the macaque (6 animal average) using protocols in the F99 standard space and protocols in the NMT standard space. All MIPs are across a window (20% of the field of view) centred at the displayed slices. Thresholded path distributions are displayed with a low threshold of 0.1% (for the EmC parts the* 90th *percentile was used).*

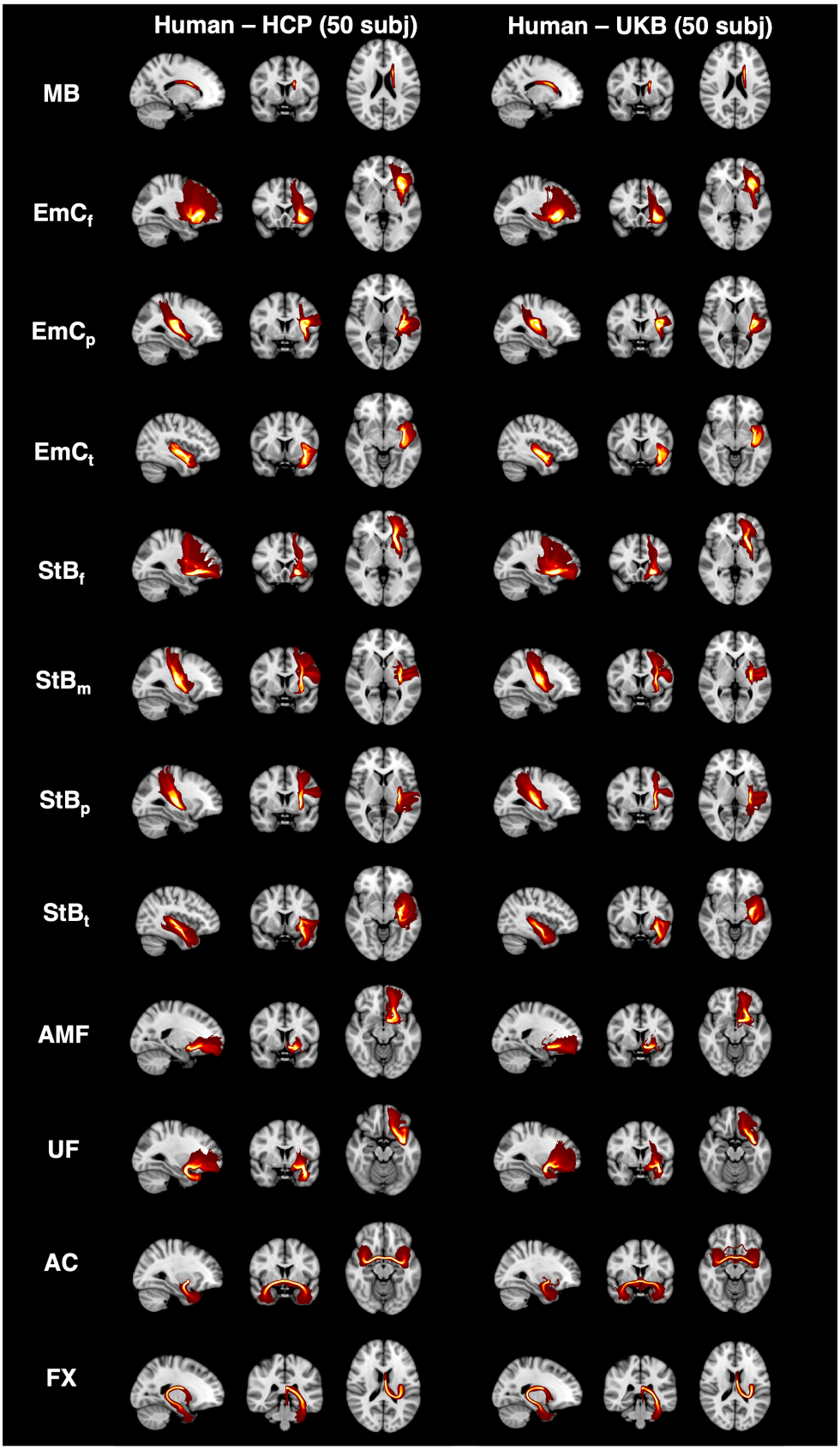

***Figure S4**: Corresponding tract reconstructions using our cortico-subcortical protocols, between different data resolutions (spatial and angular) and acquisition protocols.*. *Maximum intensity projections (MIPs) of the group-averaged path distributions for all developed tractography results for all developed protocols in 50 Human Connectome Project (HCP) and 50 UK Biobank (UKB) subjects. All MIPs are across a window (20% of the field of view) centred at the displayed slices. Thresholded path distributions are displayed with a low threshold of 0.1% (for the EmC parts the* 90th *percentile was used).*

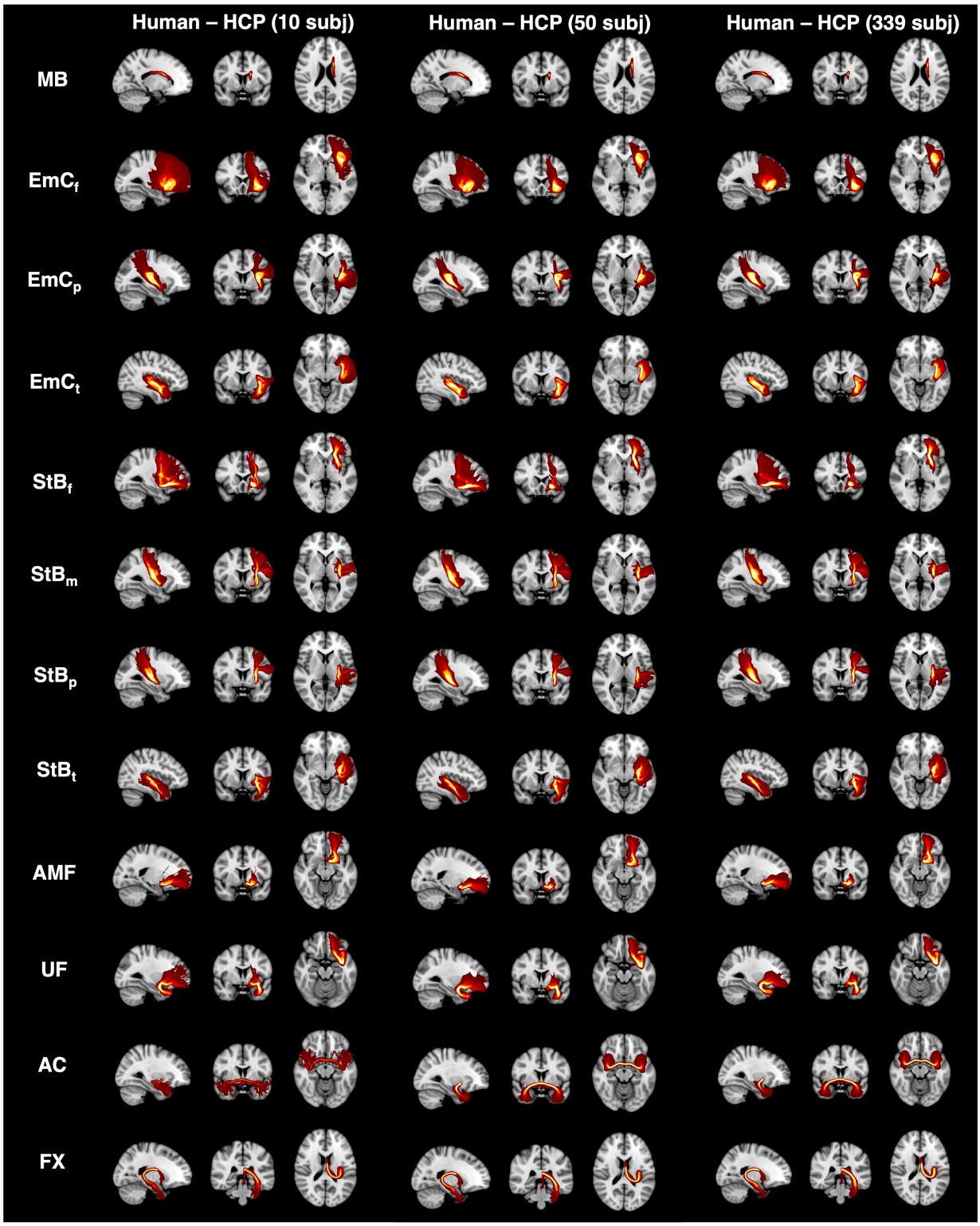

***Figure S5**: Corresponding tract reconstructions using our cortico-subcortical protocols, across different cohort sizes.*. *Maximum intensity projections (MIPs) of the group-averaged path distributions for all developed tractography results for all developed protocols in 10, 50 and 339 (all unrelated subjects) Human Connectome Project (HCP) subjects. All MIPs are across a window (20% of the field of view) centred at the displayed slices. Thresholded path distributions are displayed with a low threshold of 0.1% (for the EmC parts the* 90th *percentile was used).*

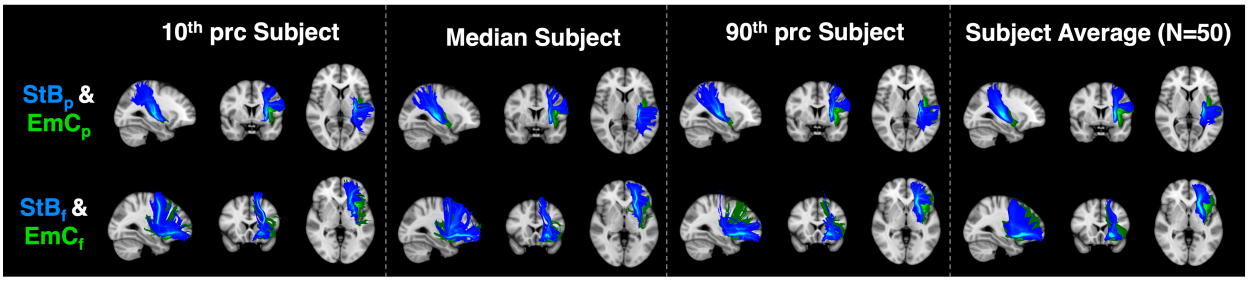

***Figure S6**: **Individual subject tract reconstructions match the group average, whilst preserving expected topology for** StB **and** EmC**.** Showing reconstruction and relative topology for frontal and parietal parts (StB_f vs EmC_f, StB_p vs EmC_p) for individual subjects. The subjects chosen are those corresponding to the 10th, 50th (median) and 90th percentile of the distribution of tract correlations against the group average for the HCP cohort (N=50). For each subject, the mean correlation to the average across all New tracts was computed and subjects were ranked based on this mean tract correlation. In all cases, tracts reconstruct similarly to the average atlas, whilst preserving the expected topology (StB more medial than EmC).*

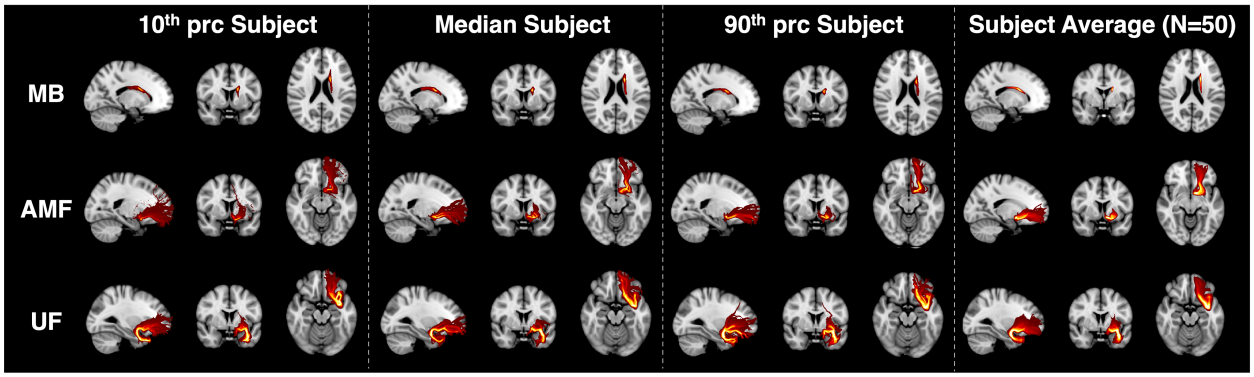

***Figure S7**: **Individual subject tract reconstructions match the group average for** MB, AMF **and** UF**.** The subjects chosen are those corresponding to the 10th, 50th (median) and 90th percentile of the tract correlations against the group average for the HCP cohort (N=50). For each subject, the mean correlation to the average across all New tracts was computed and subjects were ranked based on this mean tract correlation.. In all cases tracts reconstruct similarly to the atlas.*